responsible for the lack of PGL/PDIM production. We constructed a type II transformant by inserting *Rv3405c* or *Rv3405c-Rv3408* of RD16 in addition to type II *ppsA*, but no transformation restored the production of PGL/PDIM (data not shown). This result implies that *Rv3405c* and *Rv3405c-Rv3408* do not participate in the biosynthesis of PGL/PDIM in type II. The previous report of Chen *et al.* (22) did not describe the origin of the BCG Japan substrain, and it is unclear whether the BCG Japan they used was the same as the BCG Tokyo 172 strain used in this study. We examined the BCG Japan ATCC 35737 substrain deposited in the American Type Culture Collection (Manassas, VA) and confirmed the 22-bp deletion in *Rv3405c* and the production of PGL/PDIM (data not shown). A recent report of the genome sequence of the BCG Moreau substrain clarified that *fadD26-ppsA* (976 bp) and RD16 (7,608 bp) were deleted (28, 36). The BCG Moreau substrain is incapable of producing PGL/PDIM like BCG Tokyo 172 type II (22), and the deletion of *fadD26-ppsA* in BCG Moreau is consistent with our results. Taken together, the BCG Tokyo 172 substrain may have been divided into at least two subpopulations, types I and II, in a very early stage after it was distributed from the Pasteur Institute.

Finally, the immune effect of PGL derived from the BCG Tokyo 172 substrain was studied because type I could produce PGL but type II could not. A previous report by Reed *et al.* (37) demonstrated that the PGL of *M. tuberculosis* (PGL-tb) inhibits the innate immune response. The loss of PGL-tb was responsible for an increase in the release of TNF-α and interleukins 6 and 12 *in vitro*, and the PGL-tb-deficient mutant showed a phenotype with low virulence/pathology (37). The PGL produced by BCG substrains is the so-called mycoside B, and its sugar moiety is different from that of PGL-tb. The PGL produced by BCG substrains has only a 2-*O*-Me-Rha branch elongated from the phenol moiety, although PGL-tb has three sugar residues elongated from the phenol moiety (38). The composition of the PDIM in PGL is similar in both species. The total lipids derived from types I and II activated BMMs via TLR2 (Fig. 6). Several lipid components containing phosphatidylinositol mannosides and mycoloyl glycolipids can induce the host response via TLR2 (39, 40). Although purified PGL molecules by themselves had no effect on the activation of macrophages *in vitro*, we found that PGL suppressed the activation of BMMs elicited by total lipids. It is considered that the PGL may have a competitive inhibitory effect or may mask the active site of other TLR2 agonistic lipid components and decrease their activity. The localization of PGL/PDIM in the cell envelope of BCG substrains is critical to their biological effects.

Our present study has demonstrated differences in the lipids and biosynthesis gene cluster of PGL/PDIM of two BCG Tokyo subpopulations and their effects on the host innate immune response. Type II lacks PGL/PDIM due to a *ppsA* mutation, and this phenotype is implicated in host responses. We propose that the lipid composition in the cell envelope is important for the efficacy of a BCG vaccine. These findings shed light on the quality, safety, and efficacy of BCG, which is the only vaccine currently available against TB.

REFERENCES

1. World Health Organization (2011) *Global Tuberculosis Control 2010*, WHO Press, World Health Organization, Geneva
2. Behr, M. A. (2002) *Lancet Infect. Dis.* **2**, 86–92
3. Behr, M. A., Wilson, M. A., Gill, W. P., Salamon, H., Schoolnik, G. K., Rane, S., and Small, P. M. (1999) *Science* **284**, 1520–1523
4. Brosch, R., Gordon, S. V., Garnier, T., Eiglmeier, K., Frigui, W., Valenti, P., Dos Santos, S., Duthoy, S., Lacroix, C., Garcia-Pelayo, C., Inwald, J. K., Golby, P., Garcia, J. N., Hewinson, R. G., Behr, M. A., Quail, M. A., Churcher, C., Barrell, B. G., Parkhill, J., and Cole, S. T. (2007) *Proc. Natl. Acad. Sci. U.S.A.* **104**, 5596–5601
5. Zwerling, A., Behr, M. A., Verma, A., Brewer, T. F., Menzies, D., and Pai, M. (2011) *PLoS Med.* **8**, e1001012
6. Brosch, R., and Behr, M. A. (2005) in *Tuberculosis and the Tubercule Bacillus* (Cole, S. T., Eisenach, D. S., McMurray, D. N., and Jacobs, W. R., Jr., eds) Chapter 10, pp. 155–164, ASM Press, Washington, D. C.
7. Knezevic, I., and Corbel, M. J. (2006) *Vaccine* **24**, 3874–3877
8. Ho, M. M., Markey, K., Rigsby, P., Hockley, J., and Corbel, M. J. (2011) *Vaccine* **29**, 512–518
9. Ho, M. M., Markey, K., Rigsby, P., Jensen, S. E., Gairola, S., Seki, M., Castello-Branco, L. R., López-Vidal, Y., Knezevic, I., and Corbel, M. J. (2008) *Vaccine* **26**, 4754–4757
10. Markey, K., Ho, M. M., Choudhury, B., Seki, M., Ju, L., Castello-Branco, L. R., Gairola, S., Zhao, A., Shibayama, K., Andre, M., and Corbel, M. J. (2010) *Vaccine* **28**, 6964–6969
11. Bedwell, J., Kairo, S. K., Behr, M. A., and Bygraves, J. A. (2001) *Vaccine* **19**, 2146–2151
12. Honda, I., Seki, M., Ikeda, N., Yamamoto, S., Yano, I., Koyama, A., and Toida, I. (2006) *Vaccine* **24**, 4969–4974
13. Hayashi, D., Takii, T., Fujiwara, N., Fujita, Y., Yano, I., Yamamoto, S., Kondo, M., Yasuda, E., Inagaki, E., Kanai, K., Fujiwara, A., Kawarazaki, A., Chiba, T., and Onozaki, K. (2009) *FEMS Immunol. Med. Microbiol.* **56**, 116–128
14. Brennan, P. J., and Nikaido, H. (1995) *Annu. Rev. Biochem.* **64**, 29–63
15. Guenin-Macé, L., Siméone, R., and Demangel, C. (2009) *Transbound. Emerg. Dis.* **56**, 255–268
16. Kremer, L., de Chastellier, C., Dobson, G., Gibson, K. J., Bifani, P., Balor, S., Gorvel, J. P., Locht, C., Minnikin, D. E., and Besra, G. S. (2005) *Mol. Microbiol.* **57**, 1113–1126
17. Bhatt, A., Fujiwara, N., Bhatt, K., Gurcha, S. S., Kremer, L., Chen, B., Chan, J., Porcelli, S. A., Kobayashi, K., Besra, G. S., and Jacobs, W. R., Jr. (2007) *Proc. Natl. Acad. Sci. U.S.A.* **104**, 5157–5162
18. Gilbart, J., Fox, A., and Morgan, S. L. (1987) *Eur. J. Clin. Microbiol.* **6**, 715–723
19. Miller, L. T. (1982) *J. Clin. Microbiol.* **16**, 584–586
20. Fujiwara, N., Nakata, N., Naka, T., Yano, I., Doe, M., Chatterjee, D., McNeil, M., Brennan, P. J., Kobayashi, K., Makino, M., Matsumoto, S., Ogura, H., and Maeda, S. (2008) *J. Bacteriol.* **190**, 3613–3621
21. Naka, T., Nakata, N., Maeda, S., Yamamoto, R., Doe, M., Mizuno, S., Niki, M., Kobayashi, K., Ogura, H., Makino, M., and Fujiwara, N. (2011) *J. Bacteriol.* **193**, 5766–5774
22. Chen, J. M., Islam, S. T., Ren, H., and Liu, J. (2007) *Vaccine* **25**, 8114–8122
23. Fujiwara, N., and Kobayashi, K. (2008) in *Glycolipids: New Research* (Sasaki, M., ed) Chapter IV, pp. 99–116, Nova Science Publishers, Inc., New York
24. Sirakova, T. D., Dubey, V. S., Deb, C., Daniel, J., Korotkova, T. A., Abomoelak, B., and Kolattukudy, P. E. (2006) *Microbiology* **152**, 2717–2725
25. Guilhot, C., Chlut, C., and Daffé, M. (2008) in *The Mycobacterial Cell Envelope* (Daffé, M., and Reyrat, J.-M., eds) Chapter 17, pp. 273–288, ASM Press, Washington, D. C.
26. Behr, M. A., Schroeder, B. G., Brinkman, J. N., Slayden, R. A., and Barry,

– 78 –

C. E., 3rd. (2000) *J. Bacteriol.* **182,** 3394–3399

27. Yuan, Y., Zhu, Y., Crane, D. D., and Barry, C. E., 3rd. (1998) *Mol. Microbiol.* **29,** 1449–1458
28. Gomes, L. H., Otto, T. D., Vasconcellos, E. A., Ferrão, P. M., Maia, R. M., Moreira, A. S., Ferreira, M. A., Castello-Branco, L. R., Degrave, W. M., and Mendonça-Lima, L. (2011) *J. Bacteriol.* **193,** 5600–5601
29. Seki, M., Honda, I., Fujita, I., Yano, I., Yamamoto, S., and Koyama, A. (2009) *Vaccine* **27,** 1710–1716
30. Barrow, W. W., and Brennan, P. J. (1982) *J. Bacteriol.* **150,** 381–384
31. Etienne, G., Laval, F., Villeneuve, C., Dinadayala, P., Abouwarda, A., Zerbib, D., Galamba, A., and Daffé, M. (2005) *Microbiology* **151,** 2075–2086
32. Martínez, A., Torello, S., and Kolter, R. (1999) *J. Bacteriol.* **181,** 7331–7338
33. Scherman, H., Kaur, D., Pham, H., Skovierová, H., Jackson, M., and Brennan, P. J. (2009) *J. Bacteriol.* **191,** 6769–6772
34. Camacho, L. R., Constant, P., Raynaud, C., Laneelle, M. A., Triccas, J. A., Gicquel, B., Daffe, M., and Guilhot, C. (2001) *J. Biol. Chem.* **276,** 19845–19854
35. Rousseau, C., Winter, N., Pivert, E., Bordat, Y., Neyrolles, O., Avé, P., Huerre, M., Gicquel, B., and Jackson, M. (2004) *Cell. Microbiol.* **6,** 277–287
36. Leung, A. S., Tran, V., Wu, Z., Yu, X., Alexander, D. C., Gao, G. F., Zhu, B., and Liu, J. (2008) *BMC Genomics* **9,** 413
37. Reed, M. B., Domenech, P., Manca, C., Su, H., Barczak, A. K., Kreiswirth, B. N., Kaplan, G., and Barry, C. E., 3rd. (2004) *Nature* **431,** 84–87
38. Siméone, R., Léger, M., Constant, P., Malaga, W., Marrakchi, H., Daffé, M., Guilhot, C., and Chalut, C. (2010) *FEBS J.* **277,** 2715–2725
39. Geisel, R. E., Sakamoto, K., Russell, D. G., and Rhoades, E. R. (2005) *J. Immunol.* **174,** 5007–5015
40. Gilleron, M., Quesniaux, V. F., and Puzo, G. (2003) *J. Biol. Chem.* **278,** 29880–29889

Structure and Host Recognition of Serotype 13 Glycopeptidolipid from *Mycobacterium intracellulare*[∇][†]

Takashi Naka,[1,2][‡] Noboru Nakata,[3][‡] Shinji Maeda,[4][‡] Reina Yamamoto,[1,5] Matsumi Doe,[6]
Seiko Mizuno,[1,5] Mamiko Niki,[1] Kazuo Kobayashi,[7] Hisashi Ogura,[1,8]
Masahiko Makino,[3] and Nagatoshi Fujiwara[1]*

*Departments of Bacteriology[1] and Virology,[8] Osaka City University Graduate School of Medicine, Osaka 545-8585, Japan;
MBR Co. Ltd., Osaka 560-8552, Japan[2]; Department of Mycobacteriology, Leprosy Research Center, National Institute of
Infectious Diseases, Tokyo 189-0002, Japan[3]; Molecular Epidemiology Division, Mycobacterium Reference Center,
The Research Institute of Tuberculosis, Japan Anti-Tuberculosis Association, Tokyo 204-8533, Japan[4];
Department of Development Nourishment, Faculty of Human Development, Soai University, Osaka 559-0003,
Japan[5]; Department of Chemistry, Graduate School of Science, Osaka City University, Osaka 558-8585,
Japan[6]; and Department of Immunology, National Institute of Infectious Diseases,
Tokyo 162-8640, Japan[7]*

The *Mycobacterium avium-M. intracellulare* complex (MAIC) is divided into 28 serotypes by a species-specific glycopeptidolipid (GPL). Previously, we clarified the structures of serotype 7 GPL and two methyltransferase genes (*orfA* and *orfB*) in serotype 12 GPL. This study elucidated the chemical structure, biosynthesis gene, and host innate immune response of serotype 13 GPL. The oligosaccharide (OSE) structure of serotype 13 GPL was determined to be 4-2′-hydroxypropanoyl-amido-4,6-dideoxy-β-hexose-(1→3)-4-O-methyl-α-L-rhamnose-(1→3)-α-L-rhamnose-(1→3)-α-L-rhamnose-(1→2)-α-L-6-deoxy-talose by using chromatography, mass spectrometry, and nuclear magnetic resonance (NMR) analyses. The structure of the serotype 13 GPL was different from those of serotype 7 and 12 GPLs only in O-methylations. We found a relationship between the structure and biosynthesis gene cluster. *M. intracellulare* serotypes 12 and 13 have a 1.95-kb *orfA-orfB* gene responsible for 3-O-methylation at the terminal hexose, *orfB*, and 4-O-methylation at the rhamnose next to the terminal hexose, *orfA*. The serotype 13 *orfB* had a nonfunctional one-base missense mutation that modifies serotype 12 GPL to serotype 13 GPL. Moreover, the native serotype 13 GPL was multiacetylated and recognized via Toll-like receptor 2. The findings presented here imply that serotypes 7, 12, and 13 are phylogenetically related and confirm that acetylation of the GPL is necessary for host recognition. This study will promote better understanding of the structure-function relationships of GPLs and may open a new avenue for the prevention of MAIC infections.

The increase of drug-resistant mycobacteria and the number of immunocompromised hosts including the HIV epidemic are important problems. The *Mycobacterium avium-M. intracellulare* complex (MAIC) is distributed ubiquitously in the environment and is the most common isolate of nontuberculous mycobacteria, which are now one of the most important environmental pathogen-disseminated infectious agents in both immunocompromised and immunocompetent hosts (26, 31, 39).

The most characteristic feature of mycobacteria is richness in lipids. These hydrophobic cell wall components contribute to the surface properties and are considered to play important roles in their pathogenesis through the host immune responses (8, 17). MAIC expresses a glycopeptidolipid (GPL) as one of the representative lipid components. Structurally, the GPL is composed of two parts, a common tetrapeptido-amino alcohol core and a serotype-specific oligosaccharide (OSE) elongated

from 6-deoxy-talose (6-d-Tal). D-Phenylalanine-D-*allo*-threonine-D-alanine-L-alaninol (D-Phe-D-*allo*-Thr-D-Ala-L-alaninol), which is modified with an amido-linked 3-hydroxy or 3-methoxy C_{26}-C_{34} fatty acid at the N terminus of D-Phe, and D-*allo*-Thr and terminal L-alaninol are further linked to a 6-d-Tal and 3,4-di-O-methyl rhamnose (3,4-di-O-Me-Rha), respectively. This portion is called the serotype-nonspecific GPL (apolar GPL). Serotype-specific GPLs (polar GPLs) are produced by extending individual OSE residues from the 6-d-Tal. MAIC species are divided into 28 serotypes by serological reaction and distinctive patterns of polar GPLs on thin-layer chromatography (TLC) (7, 38). The GPL is considered to play crucial roles in the physiology of the bacteria and the host responses to MAIC infection. Several biological and immunological functions of GPLs have been reported (9, 34), but the roles of GPLs are not fully elucidated. Recently, several genes involved in GPL biosynthesis have been characterized (10, 29). To better understand the biological functions and significance of GPLs, we need to clarify the structure and biosynthetic pathways of GPLs.

The chemical structures of only 16 GPLs have been defined (9). Recently, we determined the structures of the serotype 7 and 16 GPLs and identified the gene clusters completing the OSE biosynthesis (13, 14). In addition, two methyltransferase genes of serotype 7- and 12-specific GPL biosynthesis were

---

* Corresponding author. Mailing address: Department of Bacteriology, Osaka City University Graduate School of Medicine, 1-4-3 Asahimachi, Abeno-ku, Osaka 545-8585, Japan. Phone: 81 6 6645 3746. Fax: 81 6 6645 3747. E-mail: fujiwara@med.osaka-cu.ac.jp.
† Supplemental material for this article may be found at http://jb.asm.org/.
‡ These authors contributed equally to this work.
∇ Published ahead of print on 19 August 2011.

characterized (30). In this process, we found that the structure of the serotype 13 GPL is close to that of the serotype 7 and 12 GPLs. In epidemiological serotyping, Tsang et al. (37) showed that clinical isolates of serotypes 7, 12, and 13 were found in around 10% of non-AIDS patients. However, it was difficult to distinguish serotypes 7, 12, and 13 by only serological and chromatographic techniques because of their structural similarity. The phylogeny of some MAIC strains based on GPL biosynthesis genes has been reported (23). In this study, the complete structure of the serotype 13 GPL was determined, and the genetic relationship between the serotype 7, 12, and 13 GPL biosynthesis was clarified. Moreover, the host innate immune recognition of antigenic serotype 13 GPL and the importance of structural modification were shown. We discuss the phylogeny of MAIC strains on the basis of these GPL biosynthesis genes and the relationship between GPL structure and immunogenicity.

MATERIALS AND METHODS

Bacterial strains and preparation of GPL. *M. intracellulare* serotype 13 (ATCC 35769, ATCC 25122), serotype 7 (ATCC 35847), and serotype 12 (ATCC 35762) strains were purchased from the American Type Culture Collection (Manassas, VA). The GPL preparation was performed as described previously (14, 18). Each strain of *M. intracellulare* was grown on Middlebrook 7H11 agar (Difco Laboratories, Detroit, MI) with 0.5% glycerol and 10% Middlebrook oleic acid-albumin-dextrose-catalase (OADC) enrichment (Difco) at 37°C for 2 to 3 weeks. The heat-killed bacteria were sonicated, and crude lipids were extracted with chloroform-methanol (2:1 [vol/vol]). The crude lipids were hydrolyzed with 0.2 N sodium hydroxide in methanol at 37°C for 2 h, followed by neutralization with 6 N hydrochloric acid. Alkaline-stable lipids were partitioned by a two-layer system with chloroform-methanol (2:1 [vol/vol]) and water. The organic phase was evaporated and precipitated with acetone to remove any acetone-insoluble components. The supernatant was washed (chloroform-methanol, 95:5 [vol/vol]) and eluted (chloroform-methanol, 1:1 [vol/vol]) with a Sep-Pak silica cartridge (Waters Corporation, Milford, MA) for partial purification. The GPL was completely purified by preparative TLC of Silicagel G (Uniplate; 20 by 20 cm, 250 μm; Analtech, Inc., Newark, DE). The TLC plate was developed with chloroform-methanol-water (65:25:4 and 60:16:2 [vol/vol/vol]), until a single spot was obtained. The TLC plate was sprayed with 20% sulfuric acid in ethanol and was charred at 180°C for 3 min. The GPL was detected as a brownish-yellow spot. To recover the GPL, the TLC plate was exposed to iodine vapor, and the GPL spot was marked. The silica gels of the GPL spot were scraped off, and the GPL was eluted with chloroform-methanol (2:1 [vol/vol]). The native GPL was purified by the same method as the alkaline-stable GPL, omitting the hydrolysis with 0.2 N sodium hydroxide.

Preparation of OSE moiety. β-Elimination of the GPL was performed with alkaline borohydride, and the OSE elongated from D-*allo*-Thr was released (14, 18). The GPL was stirred in a solution of equal volumes of ethanol and 10 mg/ml sodium borodeuteride in 0.5 N sodium hydroxide at 60°C for 16 h. The reaction mixture was decationized with Dowex 50W X8 beads (Dow Chemical Company, Midland, MI) and evaporated under nitrogen to remove boric acid. After partition into two layers of chloroform-methanol (2:1 [vol/vol]) and water, the upper aqueous phase was recovered and evaporated, and the OSE was purified as an oligoglycosyl alditol.

MALDI-TOF MS and MALDI-TOF MS/MS. The molecular species of the intact GPL was determined by the matrix-assisted laser desorption ionization–time of flight mass spectrometry (MALDI-TOF MS) with an Ultraflex II (Bruker Daltonics, Billerica, MA). One microgram of the GPL-dissolved chloroform-methanol (2:1 [vol/vol]) was applied to the target plate, and 1 μl of 10 mg/ml 2,5-dihydroxybenzoic acid in chloroform-methanol (1:1 [vol/vol]) was added as a matrix. The intact GPL was analyzed in the Reflectron mode with an accelerating voltage operating in positive mode at 20 kV (4). Then, the fragment pattern of the OSE was analyzed with the MALDI-TOF MS/MS mode. The OSE and 10 mg/ml 2,5-dihydroxybenzoic acid was dissolved in ethanol-water (3:7 [vol/vol]) and applied to the target plate according to the method for intact GPL.

GC/MS of carbohydrates. To determine the glycosyl composition and linkage position, gas chromatography/mass spectrometry (GC/MS) of partially methyl-ated alditol acetate derivatives was performed. Perdeuteromethylation was con-
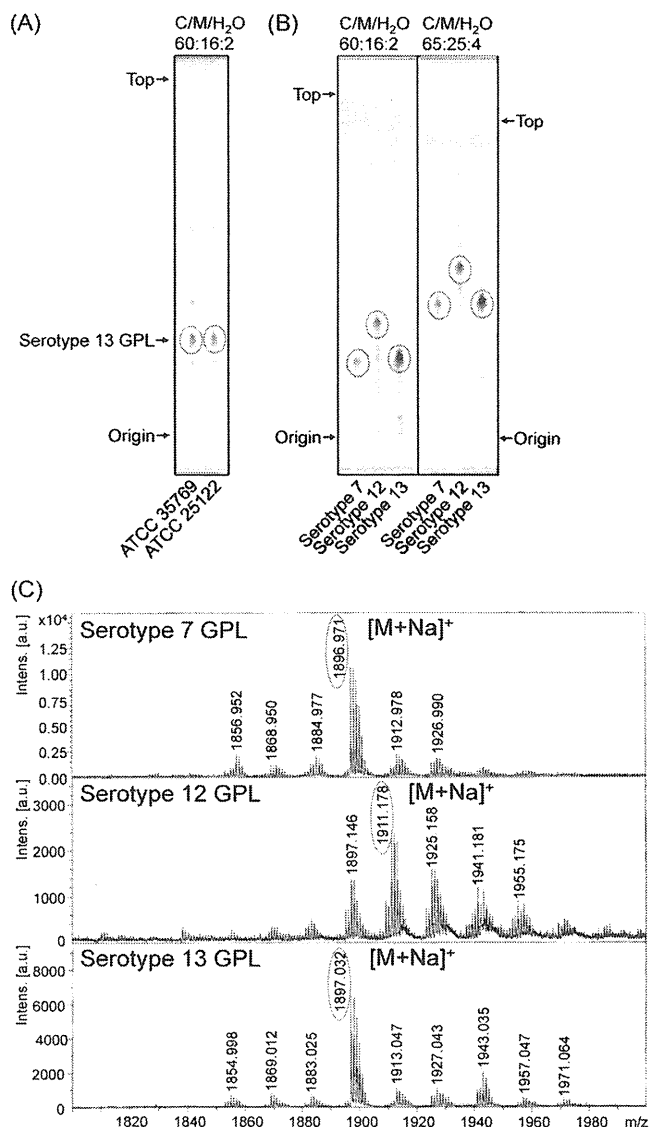

FIG. 1. TLC patterns and MALDI-TOF MS spectra of serotype 7, 12, and 13 GPLs. (A and B) The alkaline-stable lipids derived from *M. intracellulare* serotype 13 ATCC 35769 and ATCC 25122 (A) and the purified serotype 7, 12, and 13 GPLs (B) were developed on TLC plates with solvent systems of chloroform-methanol-water (60:16:2 and 65:25:4 [vol/vol/vol]). (C) The MALDI-TOF MS spectra of serotype 7, 12, and 13 GPLs were acquired using 10 mg/ml 2,5-dihydroxybenzoic acid in chloroform-methanol (1:1 [vol/vol]) as a matrix, and the molecular ions were detected as [M+Na]$^+$ in positive mode. Intens., intensity; a.u., arbitrary units.

ducted by the modified procedure of Hakomori (14, 15). The OSE was dissolved with a mixture of dimethyl sulfoxide and sodium hydroxide, followed by the addition of deuteromethyl iodide. After stirring at room temperature for 15 min, the reaction mixture was separated by a two-layer system of water and chloroform. The chloroform-containing perdeuteromethylated OSE layer was collected, washed with water two times, and evaporated completely. Partially deuteromethylated alditol acetate derivatives were prepared from perdeuteromethylated OSE by hydrolysis with 2 N trifluoroacetic acid at 120°C for 2 h, reduction with 10 mg/ml sodium borodeuteride at 25°C for 2 h, and acetylation with acetic anhydride at 100°C for 1 h (14, 19). GC/MS was performed using a benchtop ion trap mass spectrometer (GCMS-QP2010 Plus; Shimadzu Corp., Kyoto, Japan) equipped with a fused capillary column (SP-2380 and Equity-1; 30 m, 0.25-mm inner diameter [ID]; Supelco, Bellefonte, PA). Helium was used
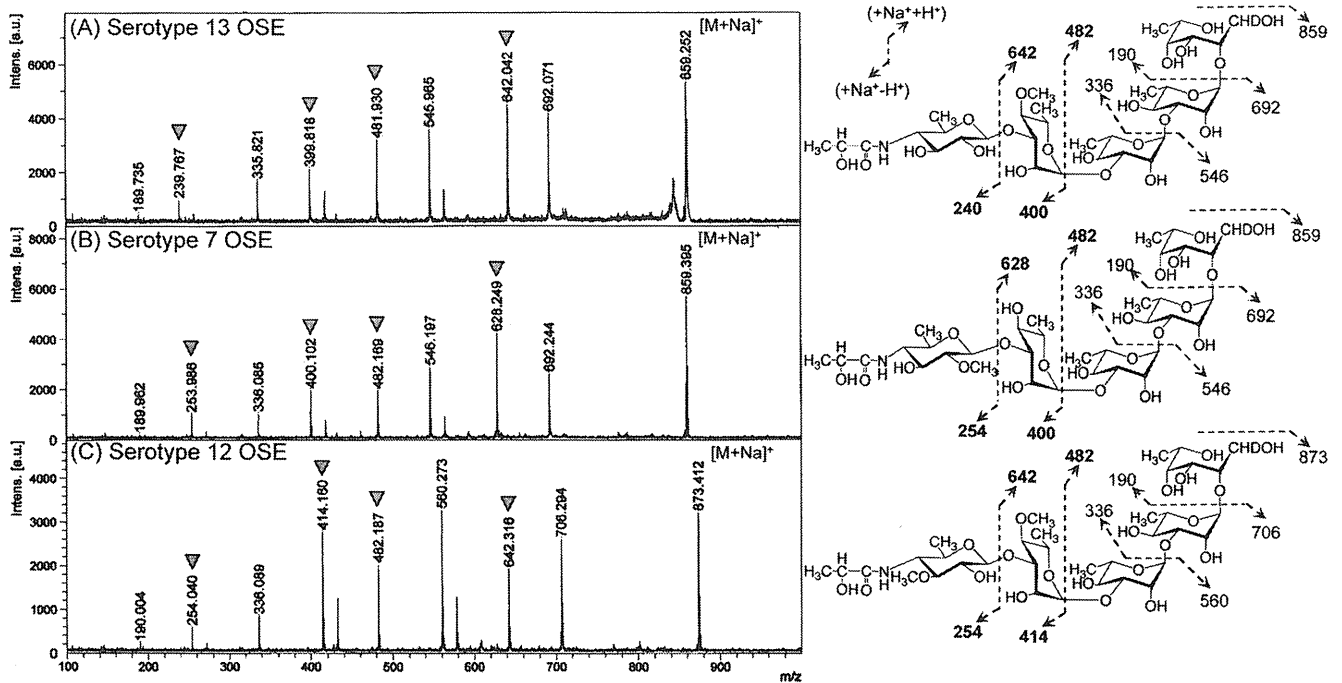
FIG. 2. MALDI-TOF MS/MS spectra of serotype 13, 7, and 12 OSEs (A, B, and C, respectively). The fragment ions by each glycosyl cleavage were detected, and the assigned fragment patterns are illustrated. Arrowheads indicate the characteristic mass numbers of the serotype 13, 7, and 12 OSEs. The matrix was 10 mg/ml 2,5-dihydroxybenzoic acid in ethanol-water (3:7 [vol/vol]), and it was performed in the MS/MS mode. Intens., intensity; a.u., arbitrary units.

as the carrier gas, and the flow rate was 1 ml/min. The temperature program for alditol acetate derivatives was started at 60°C, increased 40°C/min to 220°C, and held for 15 min, followed by an increase of 10°C/min to 260°C and holding for 10 min. The molecular separator and ion source energies were 70 eV, and the accelerating voltage was 8 kV.

NMR of GPL. The OSE was dissolved in deuterium oxide. To define the anomeric configurations of each glycosyl residue, ^{1}H and ^{13}C nuclear magnetic resonance (NMR) was employed. Both homonuclear correlation spectrometry (COSY) and ^{1}H-detected [^{1}H, ^{13}C] heteronuclear multiple-quantum correlation (HMQC) were recorded with a Bruker AVANCE-600 (Bruker BioSpin Corp. Billerica, MA), as described previously (14, 18). Ten microliters of acetone was added to the sample, and its chemical shift values, 2.04 ppm (proton) and 29.8 ppm (carbon), were used as internal controls.

Sequencing of orfA-orfB region of M. intracellulare serotype 13. PCR was used to amplify the orfA-orfB region (30) of M. intracellulare serotype 13 (ATCC 35769 and ATCC 25122), using primers orfA-F (5'-GCGGATCCAGTGTGCAGACG AGCGGAACT-3'), orfA-R (5'-GCGAATTCTTATCGAGAAAAAATAAAA G-3'), orfB-F (5'-GCGGATCCACTGCTAGACT CCGCCACCAT-3'), and orfB-R (5'-GCGAATTCCTACACCTTCACGGCGAGTC-3'). The amplified fragment was sequenced using a BigDye Terminator cycle sequencing kit, version 3.1 (Applied Biosystems, Foster City, CA), and a sequence analyzer (ABI3130xl; Applied Biosystems).

Transformation of M. intracellulare serotype 13 strain with serotype 12 orfB. The orfB fragments from serotype 12 (sero12-orfB) and serotype 13 (sero13-orfB) strains were amplified and cloned into pVV16, an expression plasmid vector for mycobacteria, downstream of the hsp60 promoter. M. intracellulare serotype 13 ATCC 35769 was transformed with pVV16-sero12-orfB and pVV16-sero13-orfB by electroporation, and hygromycin- and kanamycin-resistant colonies were isolated. Alkaline-stable lipids were prepared from heat-killed bacteria, and productive GPLs were identified by TLC, MALDI-TOF MS, MALDI-TOF MS/MS, and GC/MS.

Host recognition of native and alkaline-treated serotype 13 GPLs. The host recognition of GPLs was estimated by activations of HEK-blue-2 and -4 cells (InvivoGen, San Diego, CA). HEK-blue-2 and -4 cells are HEK293 cells stably transfected with multiple genes for recognition of Toll-like receptor 2 (TLR2) and TLR4 (including the coreceptors MD2 and CD14). In addition, HEK-blue-2 and -4 cells stably express an optimized alkaline phosphatase gene engineered to

be secreted (sAP) and placed under the control of a promoter inducible by several transcription factors, such as NF-κB and alkaline phosphatase-1. HEK-blue-2 and -4 cells were seeded at a concentration of 2×10^5 cells/ml in 96-well flat-bottom tissue culture plates and incubated with Dulbecco's modified Eagle's medium (DMEM) containing 10% fetal bovine serum (FBS) at 37°C in an atmosphere of 5% CO_2 for 3 days. The adherent HEK-blue-2 and -4 cells were stimulated by native and alkaline-treated serotype 13 GPLs. After 24 h of incubation, NF-κB activation was assayed by the levels of sAP in the supernatant. The sAP was measured in duplicate using QUANTI-Blue (InvivoGen) according to the manufacturer's instructions. As positive controls, we used lipopolysaccharide (LPS) from Escherichia coli 055:B5 (Sigma-Aldrich, St. Louis, MO) for TLR4 and Pam3CSK4 (InvivoGen) for TLR2. Two independent experiments were performed.

Nucleotide sequence accession number. The nucleotide sequence reported here has been deposited in the NCBI GenBank database under accession number AB557690.

RESULTS

Purification and molecular weight of intact GPL. The serotype 13 GPLs from M. intracellulare ATCC 35769 and 25122 were detected as spots on TLC plates and showed the same R_f value (Fig. 1A). Because serotype 13 GPL was predicted to be very close structurally to the serotype 7 and 12 GPLs, the R_f values were compared on TLC plates developed with two different chloroform-methanol-water solvent systems (65:25:4 and 60:16:2 [vol/vol/vol]), respectively. Interestingly, the R_f value of the serotype 13 GPL was lower than that of the serotype 12 GPL and almost the same as that of the serotype 7 GPL in both developing systems (Fig. 1B). The intact molecular weight of each GPL was determined. The MALDI-TOF MS spectrum of the serotype 13 GPL showed m/z 1,897 for [M+Na]$^+$ as the main molecular ion in positive mode (Fig.

1C). This mass number is identical to that of the serotype 7 GPL ([M+Na]$^+$: 1,897) and 14 atomic mass units lower than that of the serotype 12 GPL ([M+Na]$^+$: 1,911).

Glycosyl sequence of serotype 13 OSE. To determine the glycosyl sequence of the OSE, MALDI-TOF MS/MS of the oligoglycosyl alditol from serotype 13 OSE was performed. The spectrum afforded the molecular ion [M+Na]$^+$ at m/z 859, together with the characteristic mass increments in the series of glycosyloxonium ions formed on fragmentation at m/z 240, 400, 546, and 692 from the N-acylated Hex to 6-d-Tal, and at m/z 190, 336, 482, and 642 from 6-d-Tal to N-acylated Hex (Fig. 2A). In comparison, the fragment patterns of the cleaved terminal N-acylated Hex of the OSEs were m/z 254 and 628 in serotype 7 and m/z 254 and 642 in serotype 12, and those next to the terminal Hex were m/z 400 and 482 in serotype 7 and m/z 414 and 482 in serotype 12 (Fig. 2B and C). Together with the intact molecular weight of each GPL (Fig. 1B), these results strongly implied that serotype 13 GPL has no O-methyl group in the terminal N-acylated Hex but does have an O-methyl group added to the Rha next to the terminal Hex.

Carbohydrate composition and linkage analyses. GC/MS analysis of the perdeuteromethylated alditol acetate derivative from serotype 13 OSE was performed to determine the glycosyl composition. The total ion chromatography (TIC) of the GC/MS spectrum of serotype 13 GPL derivatives was compared to those of serotype 7 and 12 GPL derivatives (Fig. 3A). Previous reports showed that the carbohydrate compositions of the serotype 7 GPL were 6-d-Tal, Rha, and 4-2'-hydroxy-propanoyl-amido-3,6-dideoxy-2-O-Me-Hex, and those of the serotype 12 GPL were 6-d-Tal, Rha, 4-O-Me-Rha, and 4-2'-hydroxypropanoyl-amido-3,6-dideoxy-3-O-Me-Hex (5, 13). Comparison of the retention times and mass spectra of GC/MS determined that serotype 13 GPL was composed of 6-d-Tal, Rha, 4-O-Me-Rha, and another terminal N-acylated Hex. As shown in Fig. 3B, the perdeuteromethylated alditol acetate derivative of the terminal N-acylated Hex was assigned to 2,3-di-O-deuteromethyl-1,5-di-O-acetyl-4-2'-O-deuteromethyl-propanoyl-deuteromethylamido-4,6-dideoxy-hexitol from the fragment pattern (m/z 62, 108, 121, 168, 209, 222, 269, and 303). These results confirmed that the O-methyl group was deleted from the terminal N-acylated Hex and added to the C-4 position at Rha next to the terminal Hex. Taken together, these results established the sequence and linkage arrangement of 4-2'-hydroxypropanoyl-amido-4,6-dideoxy-Hex-(1→3)-4-O-Me-Rha-(1→3)-L-Rha-(1→3)-L-Rha-(1→2)-6-d-Tal exclusively.

NMR analysis of serotype 13 OSE. The ^{1}H NMR and ^{1}H-^{1}H homonuclear COSY analyses of the OSE derived from the serotype 13 GPL revealed four distinct anomeric protons with corresponding H1-H2 cross-peaks in the low-field region at δ4.88, 4.71, 4.97 (J_{1-2} = 1 to 2 Hz, indicative of α-anomers), and 4.52 (a doublet, J_{1-2} = 7.9 Hz, indicative of a β-hexosyl unit). When further analyzed by ^{1}H-detected [^{1}H-^{13}C] two-dimensional HMQC, the anomeric protons resonating at δ4.88, 4.71, 4.97, and 4.52 had C-1s resonating at δ102.10, 93.50, 94.00, and 103.40, respectively. The J_{CH} values for each of these protons were calculated to be 170, 170, 171, and 161 Hz by measurement of the inverse-detection nondecoupled two-dimensional HMQC (see Fig. S1 and Table S1 in the supplemental material). It was concluded that two Rha and

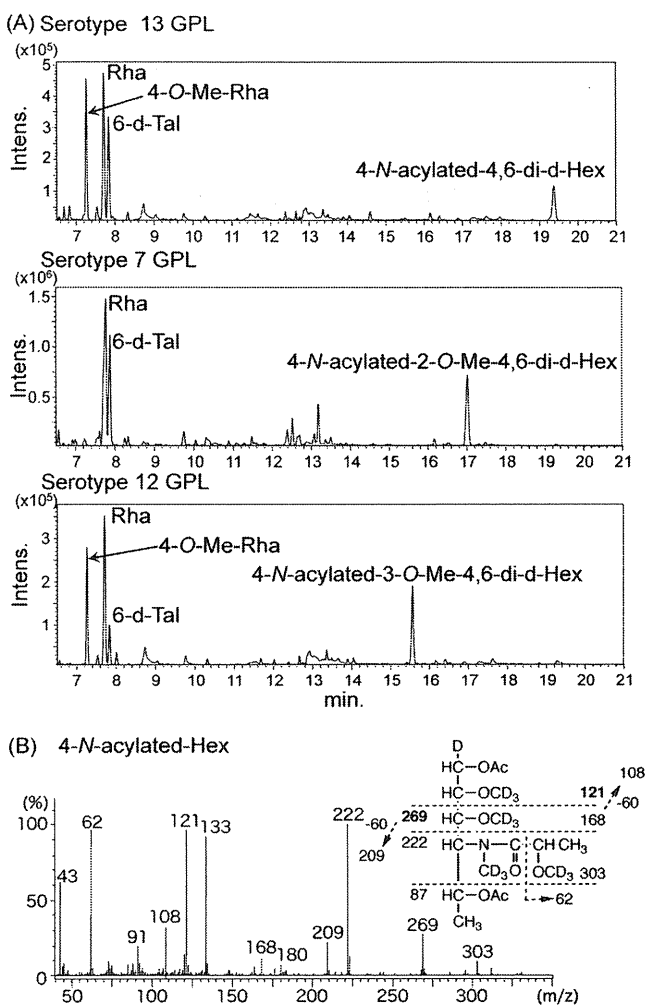(A) Serotype 13 GPL

(B) 4-N-acylated-Hex

FIG. 3. Assignment of glycosyl composition of OSEs in serotype 13 GPL. (A) Total ion chromatogram of the alditol acetate derivatives from serotype 13 compared to those of serotype 7 and 12 GPLs. A fused SP-2380 capillary column was used as the GC column. The temperature program for alditol acetate derivatives was started at 60°C, increased to 40°C/min to 220°C, and held for 15 min, followed by an increase of 10°C/min to 260°C and holding for 10 min. (B) GC/MS spectrum of the perdeuteromethylated alditol acetate derivative from the terminal Hex in serotype 13 GPL. The pattern of prominent fragment ions is illustrated. A fused Equity-1 capillary column was used as the GC column. Ac, CH$_3$CO.

4-O-Me Rha were α-anomers and that the terminal N-acylated Hex was a β configuration.

Nucleotide sequence of *orfA*-*orfB* region of *M. intracellulare* serotype 13. The present study demonstrated that the difference between the chemical structures of the serotype 13 GPL and serotype 7 and 12 GPLs was whether the O-methyl group in the terminal N-acylated Hex and the next Rha were present or not. We confirmed the genetic basis of these O-methylations. Our previous study clarified three unique open reading frames (ORFs) for methyltransferase, named *orf2*, derived from *M. intracellulare* serotype 7, and *orfA* and *orfB*, from *M. intracellulare* serotype 12 (13, 30). *orfA* and *orfB* in *M. intracellulare* serotype 12 are responsible for 4-O-methylation of the Rha next to the terminal Hex and 3-O-methylation of the
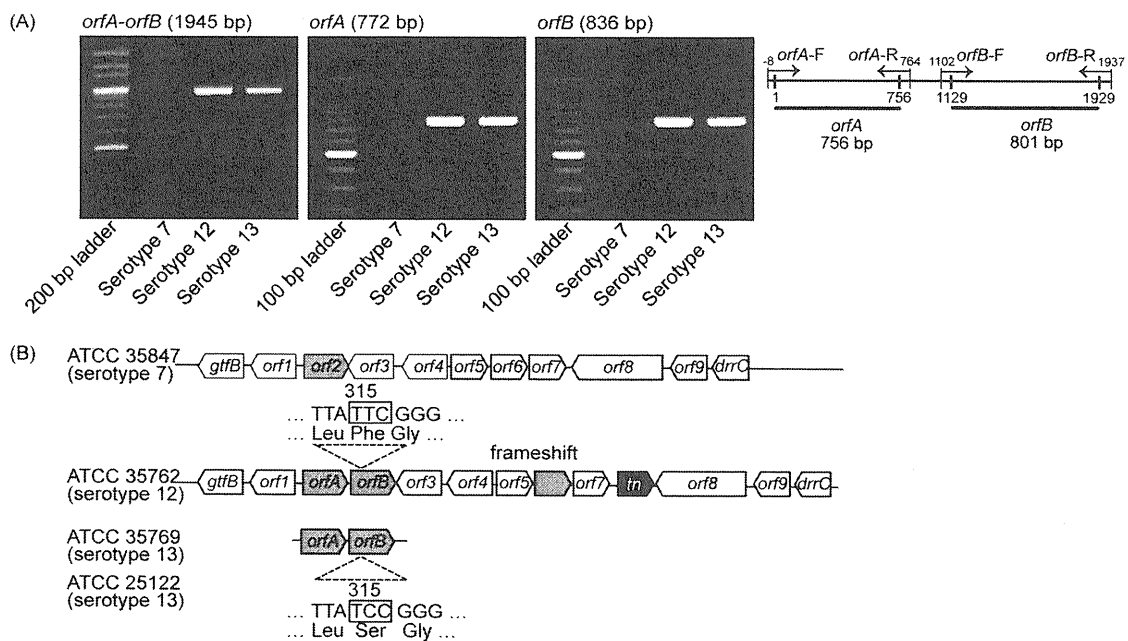
FIG. 4. Detection of *orfA-orfB* regions and comparison of genetic maps of GPL biosynthetic cluster. (A) PCR was performed to amplify the *orfA-orfB* regions of *M. intracellulare* serotype 7, 12, and 13 strains. The primers and the amplified regions are indicated. (B) *M. intracellulare* serotype 7 ATCC 35847 and serotype 12 ATCC 35762 were sequenced in our previous work (13, 30). *M. intracellulare* serotype 13 ATCC 35769 and ATCC 25122 were sequenced in this study. The missense mutation of *orfA-orfB* regions is indicated.

terminal Hex, respectively. Therefore, we examined whether or not *M. intracellulare* serotype 13 has these ORFs. First, comparison of the *gtfB-drrC* gene cluster in *M. intracellulare* serotype 7 and 12 strains implied that *orf2* in *M. intracellulare* serotype 7 replaced *orfA-orfB* in *M. intracellulare* serotype 12. We amplified the *orfA-orfB* in the genomic DNA from *M. intracellulare* serotypes 7, 12, and 13 (Fig. 4A). Interestingly, *M. intracellulare* serotype 13 had the same-sized DNA fragment of the *orfA-orfB* region, and the nucleotide sequences were determined. The 1.95-kb *orfA-orfB* regions of the two serotype 13 strains had complete identity and showed only one nucleotide substitution from that of serotype 12: codon 105, TTC, of the *orfB* in serotype 12 was replaced by codon TCC in serotype 13 (Fig. 4B). This missense mutation induced a single amino acid substitution from Phe to Ser and implied the loss of the *orfB* activity for *O*-methylation.

Expression of sero12-*orfB* and sero13-*orfB* in *M. intracellulare* serotype 13. To test the functional activity of *orfB* in *M. intracellulare* serotypes 12 and 13, the sero12-*orfB* and sero13-*orfB* genes were introduced into the *M. intracellulare* serotype 13 strain. The 0.84-kb sero12-*orfB* and sero13-*orfB* were amplified and cloned into a pVV16 vector, and *M. intracellulare* serotype 13 ATCC 35769 was transformed with the resulting plasmids and the pVV16 vector. The alkaline-stable lipids derived from the transformants were developed on TLC plates, and the productive GPLs were compared to the spots of serotype 7, 12, and 13 GPLs (Fig. 5A). Both R_f values of the GPLs produced in the transformants with the pVV16 vector and sero13-*orfB* were identical to that of the serotype 13 GPL. However, the R_f value of the GPL produced in the transformant with sero12-*orfB* was the same as that of serotype 12 GPL. By MALDI-TOF MS, the main molecular weights of the

GPLs produced in the transformants with sero12-*orfB*, sero13-*orfB*, and the pVV16 vector were detected as *m/z* 1,911, 1,897, and 1,897, respectively, for [M+Na]$^+$ (data not shown). The fragment ions of the related glycosyl cleavage in the OSEs were analyzed by using MALDI-TOF MS/MS, and the glycosyl compositions were determined. The fragment ions of the OSEs in the pVV16 vector and sero13-*orfB* showed the same pattern as serotype 13 GPL, indicating that overexpression of sero13-*orfB* in the serotype 13 strain was not affected (Fig. 2A and 5B). The fragment ions of the OSE in sero12-*orfB*, i.e., *m/z* 254 and 414, were different from those of the OSE in sero13-*orfB*, i.e., *m/z* 240 and 400, respectively (Fig. 5B). The GC/MS spectrum of the perdeuteromethylated alditol acetate derivative of the terminal *N*-acylated Hex from sero12-*orfB* was assigned to 2-*O*-deuteromethyl-1,5-di-*O*-acetyl-4-2'-*O*-deuteromethyl-propanoyl-deuteromethylamido-4,6-dideoxy-3-*O*-methyl-hexitol from the fragment pattern (*m/z* 62, 105, 121, 165, 206, 222, 266, and 300) (Fig. 5C), which was identical to that of the serotype 12 GPL. These results demonstrated that the serotype 13 transformant with sero12-*orfB* but not sero13-*orfB* had an added *O*-methyl group at the C-3 position in the terminal Hex and that the productive GPL was completely changed from serotype 13 to serotype 12. In addition, we confirmed that the plasmid-deleted C-terminal 40-base region of sero12-*orfB* was completely functional and that sero12-*orfB* worked in the serotype 7 transformant. Taken together, these results indicated that sero13-*orfB* was inactivated by the missense mutation at codon 105 and that the serotype 13 GPL lacked *O*-methylation at the C-3 position of the terminal Hex.

Native conformation of serotype 13 GPL and host response. The native serotype 13 GPL was purified without alkaline treatment. The native serotype 13 GPLs were detected on TLC
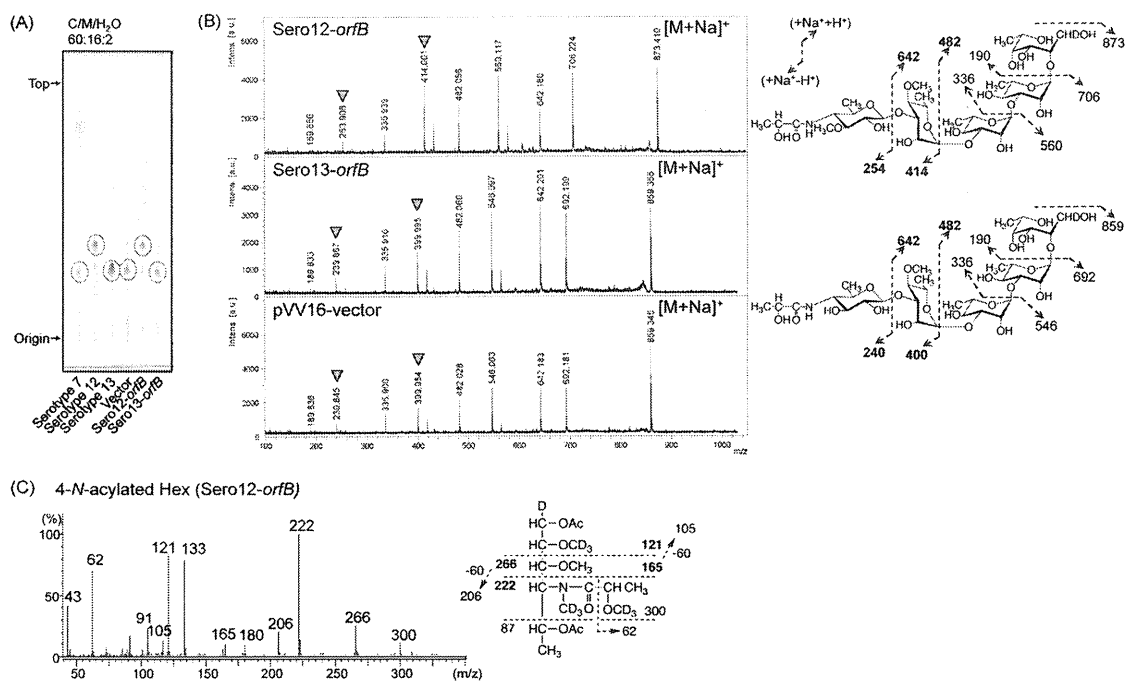
FIG. 5. The productive GPLs in transformants of *M. intracellulare* serotype 13 with sero12-*orfB* or sero13-*orfB*. (A) TLC patterns of the alkaline-stable lipids derived from *M. intracellulare* serotypes 7, 12, and 13 and serotype 13 transformants (ATCC 35769) with the pVV16-vector, sero12-*orfB*, and sero13-*orfB* from left to right, developing with a solvent system of chloroform-methanol-water (60:16:2 [vol/vol/vol]). (B) MALDI-TOF MS/MS spectra of OSEs derived from the productive GPLs in transformants of *M. intracellulare* serotype 13 with sero12-*orfB*, sero13-*orfB*, and the pVV16 vector. The replaced mass numbers are indicated by arrowheads. (C) GC/MS spectrum of the perdeuteromethylated alditol acetate derivative of the terminal *N*-acylated Hex from serotype 13 transformant with sero12-*orfB*. The MALDI TOF MS/MS and GC/MS conditions are described in the legends for Fig. 2 and 3. Ac, CH_3CO.

plates as three major spots that expanded broadly and had R_f values different from that of the alkaline-treated serotype 13 GPL. These spots were converged into one spot by alkaline treatment (Fig. 6A). It was reported that some positions of OSE in GPLs are acetylated in nature (27). The molecular weights of these three spots were checked by MALDI-TOF MS. The mass numbers of m/z 1,983, 2,025, and 2,067 for $[M+Na]^+$ caused the 2- to 4-unit increases of m/z 42 (addition of acetylations) and the modification to saturated alkyl group, compared to m/z 1,897 of the alkaline-treated serotype 13 GPL, implying that native GPLs were modified by several *O*-acetylations in the OSE portion and that alkaline treatment removed the acetylated groups (Fig. 6B). In addition, several peaks at intervals of 14 atomic mass units were caused by an alkyl group, indicating that the fatty acids of the core portion were variable and that the molecular species were heterogeneous.

To clarify the host recognitions of serotype 13 GPL via TLRs, we stimulated HEK-blue-2 and -4 cells with native and alkaline-treated serotype 13 GPLs. The native serotype 13 GPL significantly activated HEK-blue-2 cells in a dose-dependent manner, but HEK-blue-4 cells did not respond. The alkaline-treated serotype 13 GPL without *O*-acetylation did not activate either HEK-blue-2 or -4 cells. Reacetylated alkaline-treated serotype 13 GPLs with *O*-acetyl groups substituted for all hydroxy groups of OSE activated HEK-blue-2 cells, although the level of activation was less than that of the native form (Fig. 6C). Moreover, we confirmed that only the native

serotype 13 GPL stimulated mouse bone marrow-derived macrophages via TLR2 by using C57BL/6 and TLR2 knockout mice (see Fig. S2 in the supplemental material).

DISCUSSION

The structural heterogeneity of the GPLs in MAIC species is reflected in their morphology, virulence, and pathogenicity (2, 3, 24) and may be meaningful in phylogenetic classification. Actually, epidemiological studies show that the isolates of MAIC serotypes from patients are heterogeneous and important for assessing the prognosis of pulmonary MAIC disease (25, 37). Chatterjee and Khoo (9) proposed grouping the three types of GPLs by OSE structure, and the group 2 GPLs included the serotype 12, 17, and 19 strains. The serotype 7 and 16 GPLs determined in our previous studies also belong to the group 2 GPLs (13, 14). The group 2 GPLs have in common 6-d-Tal-Rha-Rha and serotype-individual sugars elongated from the second Rha. In addition, except for the serotype 19 GPL, group 2 GPLs carry an unusual substituent, *N*-acylated amido sugar, as the terminal Hex. Aspinall et al. (1) mentioned that the terminal sugar residue of serotype 12 GPL is a derivative of viosamine (4-amino-4,6-dideoxyglucose). The structural difference between serotype 7 and 12 GPLs in group 2 was due to the functions of three methyltransferase genes, *orf2*, *orfA*, and *orfB* (13, 30). In this study, we found that the serotype 13 GPL was structurally very close to those of serotypes 7 and 12, and we determined the novel structure of
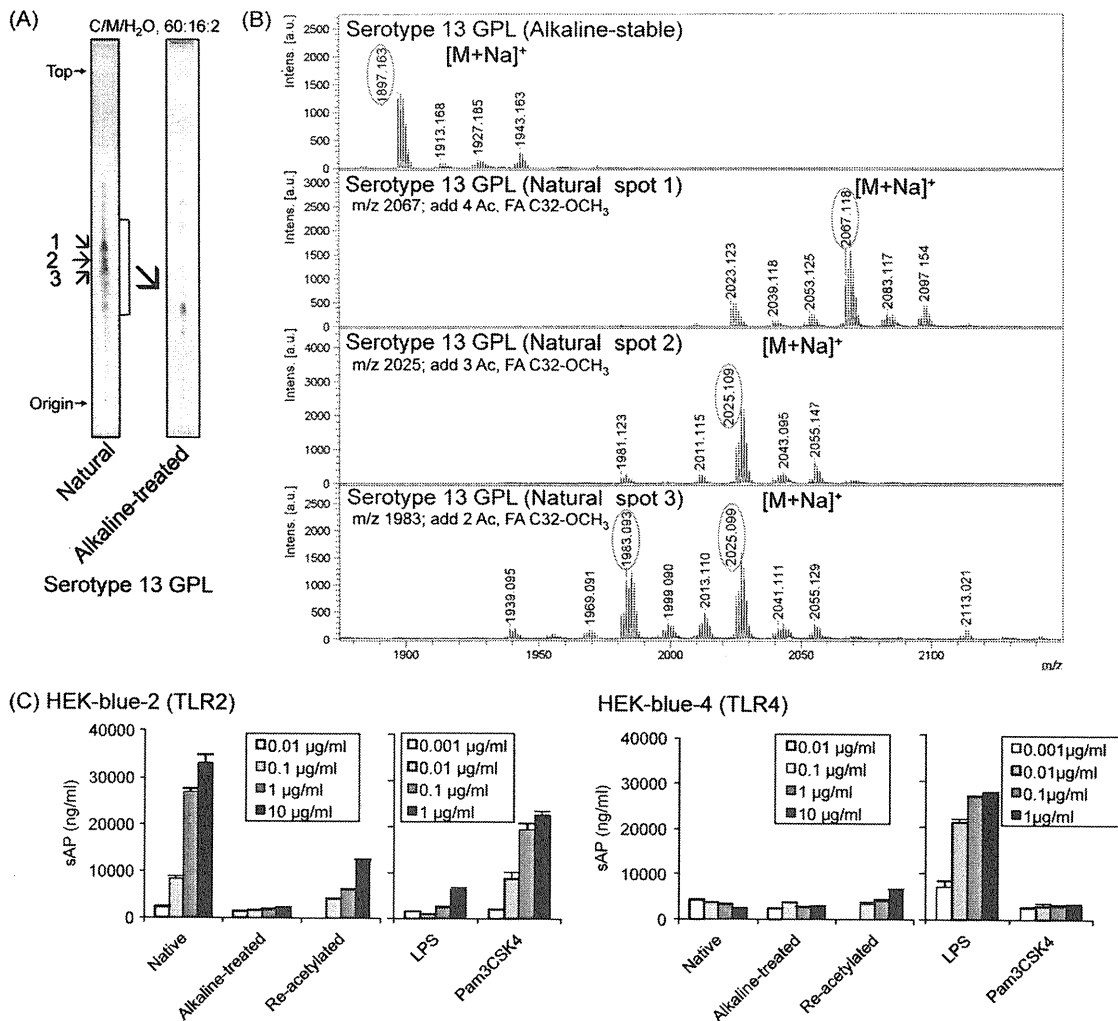
FIG. 6. TLC patterns, MALDI-TOF MS spectra, and TLR recognition of the native and alkaline-treated serotype 13 GPL. (A) The TLC plate was developed with a solvent system of chloroform-methanol-water (60:16:2 [vol/vol/vol]). Three major spots of native GPL are indicated by the numbers from top to bottom. (B) The major spots were purified and their molecular ions were measured by MALDI-TOF MS. The condition is described in the legend for Fig. 1. (C) HEK-blue-2 and -4 cells (2 × 10⁵ cells/ml) were stimulated with native, alkaline-treated, and reacetylated serotype 13 GPLs. After 24 h of incubation, NF-κB activation was assessed by measuring the levels of secreted alkaline phosphatase (sAP) in the supernatant by using QUANTI-Blue. The data are means ± standard deviations (SD) for two experiments done in duplicate.

the serotype 13 GPL to be 4-2′-hydroxypropanoyl-amido-4,6-dideoxy-β-hexose-(1→3)-4-O-methyl-α-L-rhamnose-(1→3)-α-L-rhamnose-(1→3)-α-L-rhamnose-(1→2)-α-L-6-deoxy-talose. This result clarified that the serotype 13 GPL is structurally different from the serotype 7 and 12 GPLs in the O-methylations of the terminal N-acylated Hex and Rha next to the terminal Hex. Serotype 13 GPL lacked the O-methyl group in the terminal N-acylated Hex, although serotype 7 and 12 GPLs had one at the C-2 and C-3 positions, respectively. The composition and position of the N-acyl group at the terminal Hex were completely identical in these three GPLs. At the Rha next to the terminal Hex, serotype 12 and 13 GPLs have an O-methyl group at the C-4 position, and this modification is present in all group 2 GPLs except for the serotype 7 GPL, suggesting that this methyl group may play a role in MAIC physiology and virulence. These results also implied that M.

intracellulare serotypes 7, 12, and 13 are very close phylogenetically.

We investigated the relationship between the structure and biosynthetic pathway and tried to verify the phylogenetic classification of serotypes 7, 12, and 13 by genetic analysis of GPL biosynthesis. We previously reported the nucleotide sequences of the gtfB-drrC region, which completely determine each serotype-specific GPL in serotypes 7 and 12 (13, 30), and found the sequence of the serotype 13 gene cluster (unpublished data). The genetic organizations of the gtfB-drrC regions in serotype 7, 12, and 13 gene clusters closely resemble each other. Seven common ORFs are conserved in gtfB-drrC clusters, suggesting that these three serotypes diverged from a common ancestor. The orfA-orfB region in serotypes 12 and 13 replaced orf2 in serotype 7. Only one nucleotide substitution was found in the 1.95-kb segment in orfA-orfB of serotypes 12
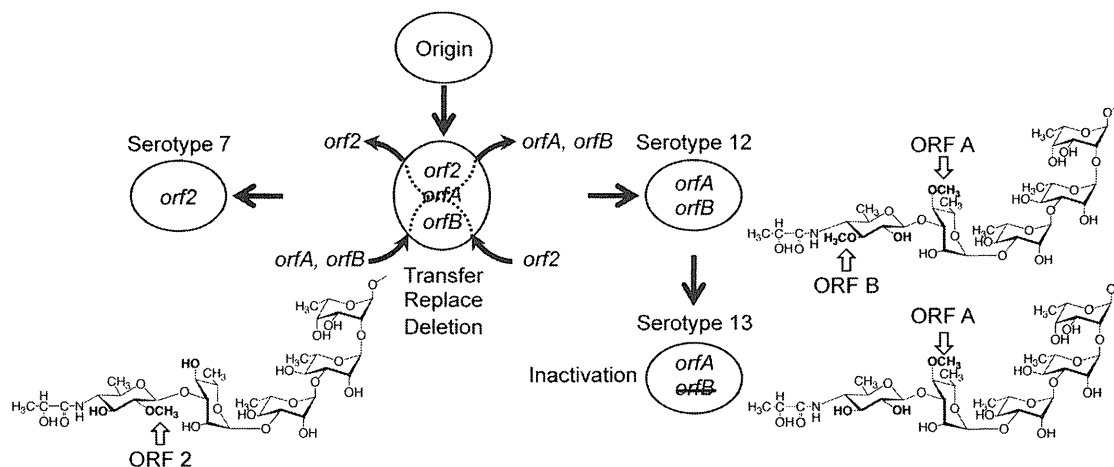
FIG. 7. Scheme of the relationship between GPL biosynthesis ORFs encoded the methyltransferases and their structures.

and 13, and *orfB* in serotype 13 was inactivated. In general, it is unusual for an ORF inactivated by a missense mutation to remain in the genome because it is a burden for the bacterium to transcribe and translate an inactivated ORF. Thus, the *M. intracellulare* serotype 13 strain must have diverged from an *M. intracellulare* serotype 12 organism recently. Serotype 13 GPL also has 4-*O*-Me-Rha. *orfA* is responsible for this methylation. In previous studies, we demonstrated that the *orfB* activity had incapacitated the *orf2* activity, which synthesizes an *O*-methyl group at the C-2 position of the terminal Hex of *M. intracellulare* serotype 7. We also showed that the *orf2* activity was independent of *orfA* activity in *M. intracellulare* serotype 12 (30). The relation of methyltransferases, *orfA*, *orfB*, and *orf2* is summarized in Fig. 7.

GPLs are correlated with colony morphology, sliding motility, biofilm formation, immune modulation, and virulence (2, 3, 16, 34). GPLs have several significant features. They are produced in MAIC species and absent from *Mycobacterium tuberculosis*, making it possible to distinguish MAIC from tuberculous mycobacteria (11, 20). An anti-GPL antibody is produced in the sera of patients and reflects the disease, which is useful in diagnosis and treatment (21, 22, 25). Moreover, it was reported that ethambutol-susceptible and -resistant MAIC strains of serotype 1 had different GPL profiles. The susceptible strain expressed only the polar serotype 1 GPL, and the resistant strain expressed several apolar GPLs. The efficacy of antibiotics may be affected by the GPL profile through differences in cell wall permeability (19). On the other hand, the importance of TLR-mediated responses has been studied in tuberculous infections. Means et al. (28) reported that *M. tuberculosis* activated both TLR2 and TLR4, whereas heat-killed *M. tuberculosis* and *M. avium* activated only TLR2. It was observed that MyD88- and TLR2-deficient mice have increased susceptibility to *M. avium* infection compared to TLR4-deficient and wild-type mice (12). These lines of evidence suggest that TLRs are related to host recognition of the MAIC components containing GPLs and affect MAIC infections. Brennan and Goren (6) first proposed that GPLs were alkaline-stable lipids and made it possible to classify serospecificity by the unique, variable deacetylated OSE sequences (9). We did not detect any biological activity of these alkaline-

treated GPLs on splenocytes and bone marrow macrophages of mice in *in vitro* stimulation. Recently, Schorey and colleagues (35, 36) clarified that serotype 1 and 2 GPLs can function as TLR2 agonists and promote macrophage activation in a TLR2- and MyD88-dependent pathway. They reported that the acetylated and methylated groups of GPLs were necessary for GPL-TLR2 interaction as a molecular requirement. In this study, we purified both native and alkaline-treated serotype 13 GPLs and clarified the acetylation patterns of serotype 13 GPL. It was confirmed that the native acetylated form of serotype 13 GPL was recognized via TLR2 and that the deacetylated form by alkaline treatment was not recognized. The serotype 13 GPL has one *O*-methyl group next to the terminal *N*-acylated Hex that was stable regardless of alkaline treatment. Taken together, an acetyl rather than a methyl group was necessary for host immune response via TLR2. The completely acetylated derivative of alkaline-treated serotype 13 GPL partially recovered the HEK-blue-2 activation, compared to the native form containing 2 to 4 acetylated groups. It may be important for GPL-TLR2 interaction to balance the hydrophobicity and hydrophilicity of the molecule. Recht and Kolter (32) reported that the acetylation of GPL affects sliding motility and biofilm formation by deleting the *atf1* gene, which is responsible for acetylation on the 6-d-Tal of GPL core in *Mycobacterium smegmatis*. Rhoades et al. (33) reported that the *Mycobacterium abscessus* GPLs were related to smooth and rough colony morphology and that the GPLs in the outermost portion of the cell wall masked underlying phosphatidyl-*myo*-inositol mannosides involved in stimulating the innate immune response via TLR2. In contrast, our results suggest that the species-specific acetylated GPL is effective in host recognition as a TLR2 agonist independent of phosphatidyl-*myo*-inositol mannosides and that it plays important roles directly in host innate immune responses. Regulating the acetylation of GPL may control the MAIC pathogenicity by, for example, developing the inhibitor of ATF1.

The present study demonstrated the chemical structure and biosynthesis gene cluster of the serotype 13 GPL of *M. intracellulare* and host innate immune response via TLR2. Serotype 13 GPL should be included in group 2 GPLs, and the phylogenetic relationship of serotype 7, 12, and 13 strains was par-

tially clarified by the GPL. We propose that the lipid components in the cell envelope are important for MAIC infection and that the structure modification must be taken into account. These findings shed light on the better understanding of the structure-function relationships of GPLs and may open a new avenue for the prevention of MAIC infections.

ACKNOWLEDGMENTS

REFERENCES

1. **Aspinall, G. O., D. Chatterjee, and P. J. Brennan.** 1995. The variable surface glycolipids of mycobacteria: structures, synthesis of epitopes, and biological properties. Adv. Carbohydr. Chem. Biochem. **51:**169–242.
2. **Belisle, J. T., K. Klaczkiewicz, P. J. Brennan, W. R. Jacobs, Jr., and J. M. Inamine.** 1993. Rough morphological variants of *Mycobacterium avium*. Characterization of genomic deletions resulting in the loss of glycopeptidolipid expression. J. Biol. Chem. **268:**10517–10523.
3. **Bhatnagar, S., and J. S. Schorey.** 2007. Exosomes released from infected macrophages contain *Mycobacterium avium* glycopeptidolipids and are proinflammatory. J. Biol. Chem. **282:**25779–25789.
4. **Bhatt, A., et al.** 2007. Deletion of kasB in *Mycobacterium tuberculosis* causes loss of acid-fastness and subclinical latent tuberculosis in immunocompetent mice. Proc. Natl. Acad. Sci. U. S. A. **104:**5157–5162.
5. **Bozic, C. M., M. McNeil, D. Chatterjee, I. Jardine, and P. J. Brennan.** 1988. Further novel amido sugars within the glycopeptidolipid antigens of *Mycobacterium avium*. J. Biol. Chem. **263:**14984–14991.
6. **Brennan, P. J., and M. B. Goren.** 1979. Structural studies on the type-specific antigens and lipids of the *Mycobacterium avium-Mycobacterium intracellulare-Mycobacterium scrofulaceum* serocomplex. *Mycobacterium intracellulare* serotype 9. J. Biol. Chem. **254:**4205–4211.
7. **Brennan, P. J., M. Heifets, and B. P. Ullom.** 1982. Thin-layer chromatography of lipid antigens as a means of identifying nontuberculous mycobacteria. J. Clin. Microbiol. **15:**447–455.
8. **Brennan, P. J., and H. Nikaido.** 1995. The envelope of mycobacteria. Annu. Rev. Biochem. **64:**29–63.
9. **Chatterjee, D., and K. H. Khoo.** 2001. The surface glycopeptidolipids of mycobacteria: structures and biological properties. Cell. Mol. Life Sci. **58:**2018–2042.
10. **Eckstein, T. M., J. T. Belisle, and J. M. Inamine.** 2003. Proposed pathway for the biosynthesis of serovar-specific glycopeptidolipids in *Mycobacterium avium* serovar 2. Microbiology **149:**2797–2807.
11. **Enomoto, K., et al.** 1998. Rapid serodiagnosis of *Mycobacterium avium-intracellulare* complex infection by ELISA with cord factor (trehalose 6, 6'-dimycolate), and serotyping using the glycopeptidolipid antigen. Microbiol. Immunol. **42:**689–696.
12. **Feng, C. G., et al.** 2003. Mice lacking myeloid differentiation factor 88 display profound defects in host resistance and immune responses to *Mycobacterium avium* infection not exhibited by Toll-like receptor 2 (TLR2)- and TLR4-deficient animals. J. Immunol. **171:**4758–4764.
13. **Fujiwara, N., et al.** 2007. Structural characterization of a specific glycopeptidolipid containing a novel *N*-acyl-deoxy sugar from *Mycobacterium intracellulare* serotype 7 and genetic analysis of its glycosylation pathway. J. Bacteriol. **189:**1099–1108.
14. **Fujiwara, N., et al.** 2008. Structural analysis and biosynthesis gene cluster of an antigenic glycopeptidolipid from *Mycobacterium intracellulare*. J. Bacteriol. **190:**3613–3621.
15. **Hakomori, S.** 1964. A rapid permethylation of glycolipid, and polysaccharide catalyzed by methylsulfinyl carbanion in dimethyl sulfoxide. J. Biochem. **55:**205–208.
16. **Howard, S. T., et al.** 2006. Spontaneous reversion of *Mycobacterium abscessus* from a smooth to a rough morphotype is associated with reduced expression of glycopeptidolipid and reacquisition of an invasive phenotype. Microbiology **152:**1581–1590.
17. **Kaufmann, S. H.** 2001. How can immunology contribute to the control of tuberculosis? Nat. Rev. Immunol. **1:**20–30.
18. **Khoo, K. H., et al.** 1996. Novel *O*-methylated terminal glucuronic acid characterizes the polar glycopeptidolipids of *Mycobacterium habana* strain TMC 5135. J. Biol. Chem. **271:**12333–12342.
19. **Khoo, K. H., et al.** 1999. Altered expression profile of the surface glycopeptidolipids in drug-resistant clinical isolates of *Mycobacterium avium* complex. J. Biol. Chem. **274:**9778–9785.
20. **Kitada, S., et al.** 2008. Serodiagnosis of *Mycobacterium avium*-complex pulmonary disease using an enzyme immunoassay kit. Am. J. Respir. Crit. Care Med. **177:**793–797.
21. **Kitada, S., et al.** 2010. Serodiagnosis of pulmonary disease due to *Mycobacterium avium* complex proven by bronchial wash culture. Chest **138:**236–237.
22. **Kitada, S., et al.** 2007. Serological test and chest computed tomography findings in patients with *Mycobacterium avium* complex lung disease. Eur. Respir. J. **29:**1217–1223.
23. **Krzywinska, E., J. Krzywinski, and J. S. Schorey.** 2004. Phylogeny of *Mycobacterium avium* strains inferred from glycopeptidolipid biosynthesis pathway genes. Microbiology **150:**1699–1706.
24. **Krzywinska, E., and J. S. Schorey.** 2003. Characterization of genetic differences between *Mycobacterium avium* subsp. *avium* strains of diverse virulence with a focus on the glycopeptidolipid biosynthesis cluster. Vet. Microbiol. **91:**249–264.
25. **Maekura, R., et al.** 2005. Clinical and prognostic importance of serotyping *Mycobacterium avium-Mycobacterium intracellulare* complex isolates in human immunodeficiency virus-negative patients. J. Clin. Microbiol. **43:**3150–3158.
26. **Marras, T. K., and C. L. Daley.** 2002. Epidemiology of human pulmonary infection with nontuberculous mycobacteria. Clin. Chest Med. **23:**553–567.
27. **Matsunaga, I., T. Komori, A. Ochi, N. Mori, and M. Sugita.** 2008. Identification of antibody responses to the serotype-nonspecific molecular species of glycopeptidolipids in *Mycobacterium avium* infection. Biochem. Biophys. Res. Commun. **377:**165–169.
28. **Means, T. K., et al.** 1999. Human Toll-like receptors mediate cellular activation by *Mycobacterium tuberculosis*. J. Immunol. **163:**3920–3927.
29. **Miyamoto, Y., et al.** 2010. Novel rhamnosyltransferase involved in biosynthesis of serovar 4-specific glycopeptidolipid from *Mycobacterium avium* complex. J. Bacteriol. **192:**5700–5708.
30. **Nakata, N., et al.** 2008. Identification and characterization of two novel methyltransferase genes that determine the serotype 12-specific structure of glycopeptidolipids of *Mycobacterium intracellulare*. J. Bacteriol. **190:**1064–1071.
31. **Primm, T. P., C. A. Lucero, and J. O. Falkinham III.** 2004. Health impacts of environmental mycobacteria. Clin. Microbiol. Rev. **17:**98–106.
32. **Recht, J., and R. Kolter.** 2001. Glycopeptidolipid acetylation affects sliding motility and biofilm formation in *Mycobacterium smegmatis*. J. Bacteriol. **183:**5718–5724.
33. **Rhoades, E. R., et al.** 2009. *Mycobacterium abscessus* glycopeptidolipids mask underlying cell wall phosphatidyl-myo-inositol mannosides blocking induction of human macrophage TNF-alpha by preventing interaction with TLR2. J. Immunol. **183:**1997–2007.
34. **Schorey, J. S., and L. Sweet.** 2008. The mycobacterial glycopeptidolipids: structure, function, and their role in pathogenesis. Glycobiology **18:**832–841.
35. **Sweet, L., and J. S. Schorey.** 2006. Glycopeptidolipids from *Mycobacterium avium* promote macrophage activation in a TLR2- and MyD88-dependent manner. J. Leukoc. Biol. **80:**415–423.
36. **Sweet, L., et al.** 2008. *Mycobacterium avium* glycopeptidolipids require specific acetylation and methylation patterns for signaling through Toll-like receptor 2. J. Biol. Chem. **283:**33221–33231.
37. **Tsang, A. Y., J. C. Denner, P. J. Brennan, and J. K. McClatchy.** 1992. Clinical and epidemiological importance of typing of *Mycobacterium avium* complex isolates. J. Clin. Microbiol. **30:**479–484.
38. **Tsang, A. Y., I. Drupa, M. Goldberg, J. K. McClatchy, and P. J. Brennan.** 1983. Use of serology and thin-layer chromatography for the assembly of an authenticated collection of serovars within the *Mycobacterium avium-Mycobacterium intracellulare-Mycobacterium scrofulaceum* complex. Int. J. Syst. Bacteriol. **33:**285–292.
39. **Wagner, D., and L. S. Young.** 2004. Nontuberculous mycobacterial infections: a clinical review. Infection **32:**257–270.

A Histone-Like Protein of Mycobacteria Possesses Ferritin Superfamily Protein-Like Activity and Protects against DNA Damage by Fenton Reaction

Masaki Takatsuka[1,2], Mayuko Osada-Oka[1], Eisuke F. Satoh[3], Kengo Kitadokoro[4], Yukiko Nishiuchi[5], Mamiko Niki[1], Masayasu Inoue[3], Kazuhiro Iwai[6], Tetsuo Arakawa[2], Yoshihiro Shimoji[7], Hisashi Ogura[8], Kazuo Kobayashi[9], Anura Rambukkana[10], Sohkichi Matsumoto[1]*

1 Department of Bacteriology, Osaka City University Graduate School of Medicine, Abeno-ku, Osaka, Japan, 2 Department of Gastroenterology, Osaka City University Graduate School of Medicine, Abeno-ku, Osaka, Japan, 3 Department of Molecular Pathology, Osaka City University Graduate School of Medicine, Abeno-ku, Osaka, Japan, 4 Department of Biomolecular Engineering, Graduate School of Science and Technology, Kyoto Institute of Technology, Matsugasakigosyokaidou-cho, Sakyo-ku, Kyoto, Japan, 5 Toneyama Institute for Tuberculosis Research, Osaka City University Medical School, Toyonaka, Osaka, Japan, 6 Department of Biophysics and Biochemistry, Graduate School of Medicine and Cell Biology and Metabolism Group, Graduate School of Frontier Biosciences, Osaka University, Suita, Osaka, Japan, 7 National Institute of Animal Health, Tsukuba, Ibaraki, Japan, 8 Department of Virology, Osaka City University Graduate School of Medicine, Abeno-ku, Osaka, Japan, 9 Department of Immunology, National Institute of Infectious Diseases, Shinjuku-ku, Tokyo, Japan, 10 Centers for Regenerative Medicine, Neuroregeneration, and Infectious Diseases, University of Edinburgh, Edinburgh, Scotland, United Kingdom

Abstract

Iron is an essential metal for living organisms but its level must be strictly controlled in cells, because ferrous ion induces toxicity by generating highly active reactive oxygen, hydroxyl radicals, through the Fenton reaction. In addition, ferric ion shows low solubility under physiological conditions. To overcome these obstacles living organisms possess Ferritin superfamily proteins that are distributed in all three domains of life: bacteria, archaea, and eukaryotes. These proteins minimize hydroxyl radical formation by ferroxidase activity that converts Fe^{2+} into Fe^{3+} and sequesters iron by storing it as a mineral inside a protein cage. In this study, we discovered that mycobacterial DNA-binding protein 1 (MDP1), a histone-like protein, has similar activity to ferritin superfamily proteins. MDP1 prevented the Fenton reaction and protects DNA by the ferroxidase activity. The K_m values of the ferroxidase activity by MDP1 of *Mycobacterium bovis* bacillus Calmette-Guérin (BCG-3007c), *Mycobacterium tuberculosis* (Rv2986c), and *Mycobacterium leprae* (ML1683; ML-LBP) were 0.292, 0.252, and 0.129 mM, respectively. Furthermore, one MDP1 molecule directly captured 81.4±19.1 iron atoms, suggesting the role of this protein in iron storage. This study describes for the first time a ferroxidase-iron storage protein outside of the ferritin superfamily proteins and the protective role of this bacterial protein from DNA damage.

Introduction

Iron is an essential element for virtually all living organisms, and is convertible between the ferrous ion (Fe^{2+}) and ferric ion (Fe^{3+}) under physiological pH. Living organisms employ this feature of iron for the catalytic centers of several critical enzymes, such as ribonucleotide reductase for the synthesis of DNA substrates and cytochromes involved in electron transport in respiration.

However, iron levels must be strictly regulated as it is potentially toxic to cells. Fe^{3+} is stable but forms insoluble hydroxy-aquo complexes and its solubility is under 10^{-18} M in physiological conditions; bacterial multiplication requires approximately 10^{-7} M iron [1]. Fe^{2+} is a reductant and generates reactive oxygen species (ROS) and reactive nitrogen species (RNS), which damage most cell components, including DNA, membranes, and proteins. In particular, the hydroxyl radical (•OH) is known as

most reactive species in ROS and toxic for the cells. The hydroxyl radical is generated via the non-enzymatic Fenton reaction:

$$Fe^{2+} + H_2O_2 \rightarrow Fe^{3+} + HO^- + \bullet OH$$
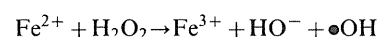
Most cells are equipped with mechanisms that protect the vital cellular components from ROS and NOS. The ferritin superfamily proteins, which are distributed among the three domains of life in both aerobic and anaerobic organisms, play a central role by detoxifying iron by converting Fe^{2+} to Fe^{3+} through its ferroxidase activity and subsequently store Fe^{3+} as a mineral. Ferritin superfamily proteins can be categorized by the presence or absence of heme. In bacteria, the former are called ferritin-like proteins or bacterioferritins and the latter are called mini-ferritins or DNA-binding protein in starved cells (Dps). Ferritin and

bacterial ferritin-like proteins have exactly the same architecture, assembling in 24 subunits to form an inner nanocage, where a maximum of 4,500 Fe^{3+} can be sequestered as mineral after been oxidized from Fe^{2+} at the ferroxidase center [2,3]. Dps forms the dodecameric oligomer and some of them possess DNA-binding activity. It similarly oxidizes Fe^{2+} at the ferroxidase center and stores a maximum 500 Fe^{3+} inside the protein [4–6].

Mycobacterium tuberculosis complex and *Mycobacterium leprae*, the etiologic agents of tuberculosis and leprosy respectively, are a serious threat to human health. According to WHO's weekly epidemiological report in 2010, tuberculosis alone kills 1.57 million people annually and 219,826 people are suffering from leprosy. These human pathogens are obligate intracellular bacteria that can survive or multiply particularly well in macrophages and Schwann cells. These invading mycobacteria restrict the host cell iron and iron-mediated ROS generation following NADPH dependent oxidative burst as efficient strategies against host defense [7]. Mycobacteria synthesize iron-chelating molecules, siderophores, and deprive the host cells of iron; they also produce antioxidant molecules, such as superoxide dismutase and catalase. Iron overload increases the risk of tuberculosis in the African human population [8] and a deficiency in siderophore synthesis prevents the replication of *M. tuberculosis* in macrophages [9]. Thus, coordination of iron homeostasis is essential to sustain survival and growth of mycobacteria in the host [10]. Both *M. tuberculosis* and *M. leprae* produce bacterioferritins [11–13], which should be involved controlling iron homeostasis of these pathogens.

DNA is an important cellular component and living organisms should be protected from damage caused by ROS. Because *M. tuberculosis* and *M. leprae* lack DNA-binding ferritin superfamily proteins like Dps [14,15], it is thought that novel molecules that have not been identified mediate DNA protection in pathogenic mycobacteria. Colangeli et al have recently shown that mycobacterial histone-like protein Lsr2 protects DNA by acting as a physical shield [16]. However, Lsr2 lacks iron-binding and ferroxidase activities [16].

Mycobacteria including *M. tuberculosis* and *M. leprae* produce mycobacterial DNA-binding protein 1 (MDP1), also designated as laminin binding protein of *M. leprae* (ML-LBP) [17,18] (Figure S1). The N- and C-terminal halves of this protein resemble bacterial histone-like proteins, IHF and HU and eukaryotic histone H1, respectively, and possesses MDP1/ML-LBP-specific DNA-binding motif (Figure S1) [17,19–21]. In this study, we found that MDP1/ML-LBP has functions of a ferritin superfamily protein, that is both ferroxidase and iron-storage activities, and protects DNA not only physically but also prevents the iron-induced Fenton reaction. To our knowledge, this is the first report of a protein capable of storing and detoxifying iron other than ferritin superfamily proteins in living organisms.

Results

MDP1/ML-LBP possesses affinity for Fe^{3+} but not Fe^{2+}

MDP1/ML-LBP mediates several cellular processes through binding to DNA, sugar-containing molecules, and proteins both inside and outside of mycobacteria [19,21–23]. Therefore we analyzed the potential interaction between MDP1 of *Mycobacterium bovis* bacillus Calmette Guérin (BCG) (BCG-MDP1) and each ligand (analyte) by measuring surface plasmon resonance (SPR) with a BIAcore 2000 biosensor. In the course of this study, we unexpectedly observed strong increase of SPR, suggesting interaction between the analyte and immobilized ligand, when Fe^{3+} (ammonium iron (III) citrate) alone was added to the BCG-

MDP1 immobilized sensor (Fig. 1A). By contrast, a gradual decrease of SPR was detected when Fe^{2+} (FeSO$_4$) was injected. Such obvious increase and decrease of SPR were not detected on injection of other metals, such as Cu^{2+}, Mg^{2+}, Mn^{2+}, and Zn^{2+} (Fig. 1A).

Resonance units (RU) analyzed by BIAcvaluation software of SPR are tightly correlated with the weight of bound protein ligand. However RU are not always correlated with weight in the case of protein-small molecule interaction [24]. In addition, it was reported that protein-metal interaction changes the protein structure, which in turn causes the changes of SPR [25]. Therefore, we next examined the binding capacity of BCG-MDP1 to Fe^{3+} by using radioactive ^{55}Fe. The results showed that ^{55}Fe bound to BCG-MDP1 but not to BSA coated on the ELISA plate (Fig. 1B). By contrast, iron pre-incubated with 10 mM ascorbic acid, which reduces Fe^{3+} to Fe^{2+}, did not interact with BCG-MDP1. In addition, the BCG-MDP1-^{55}Fe interaction was inhibited in the presence of excess amounts of cold Fe^{3+} but not Cu^{2+} (CuSO$_4$) (Fig. 1C). Taken together, these data demonstrate that BCG-MDP1 binds Fe^{3+}.

In order to determine whether the close mycobacterial MDP1-homologues have similar binding activity, we cloned the gene encoding MDP1 from *M. tuberculosis* H37Rv and purified it as a recombinant histidine-tagged protein (Mtb-MDP1) after expression in *E. coli*. Similarly, we also obtained recombinant ML-LBP of *M. leprae* after purification from *E. coli* expressing ML-LBP as described previously [18]. We analyzed the ^{55}Fe binding activities of these recombinant proteins. Like BCG-MDP1, both Mtb-MDP1 and ML-LBP bound to Fe^{3+} but not Fe^{2+} (Fig. 1D).

We next examined how many iron atoms MDP1 chelates using ICP-MS. BCG-MDP1 retained in the heparin column was incubated in the presence of 1 mM Fe^{3+} solution for 30 min and unbound iron was extensively washed. The BCG-MDP1-iron complex was eluted by 2 M NaCl and the iron content in the solution was determined by ICP-MS. The calculated data showed that one BCG-MDP1 contained 81.4 ± 19.1 iron atoms (Table 1).

MDP1/ML-LBP has ferroxidase activity

The SPR analysis showed reduction of RU when Fe^{2+} was injected into a BCG-MDP1-immobilized sensor (Fig. 1A), implying some unknown responses of MDP1 in the presence of Fe^{2+}. Although MDP1 has no motifs for ferroxidase, we next examined whether MDP1/ML-LBP has enzymatic ferroxidase bioactivity.

We performed spectral analysis at 305 nm, because ferroxidase activity is the reaction, which converts Fe^{2+} to Fe^{3+}, resulting in production of the dinuclear iron (μ-oxo-bridged Fe^{3+} dimmers). To analyze the activity, protein at a concentration of 1.4 μM was incubated at 37°C for 120 seconds in 20 mM Tris-HCl (pH 7.0). Both BCG-MDP1 and buffer alone (0.4 mM FeSO$_4$) did not absorb at 305 nm during 120 seconds incubation (Fig. 2A, broken line and dush-dotted line, respectively). In contrast, in the presence of both BCG-MDP1 and 0.4 mM FeSO$_4$ there was a rapid increase in the absorbance (Fig. 2A, solid line) with a K_m value of 0.292 mM (Fig. 3A). Similarly, the enzymatic activity of both Mtb-MDP1 and ML-LBP possess identical ferroxidase activities (Fig. 2B and 2C), of which K_m values were calculated as 0.252 mM and 0.129 mM, respectively (Fig. 3B and C). By contrast, BSA and bovine histone H1 did not show such an increase in absorbance at 305 nm (Figure S2).

MDP1/ML-LBP prevents the iron-induced Fenton reaction

Since ferroxidase activity can prevent the Fenton reaction by converting Fe^{2+} into Fe^{3+}, we examined whether MDP1 and ML-LBP could abolish the Fenton reaction. Hydroxyl radical
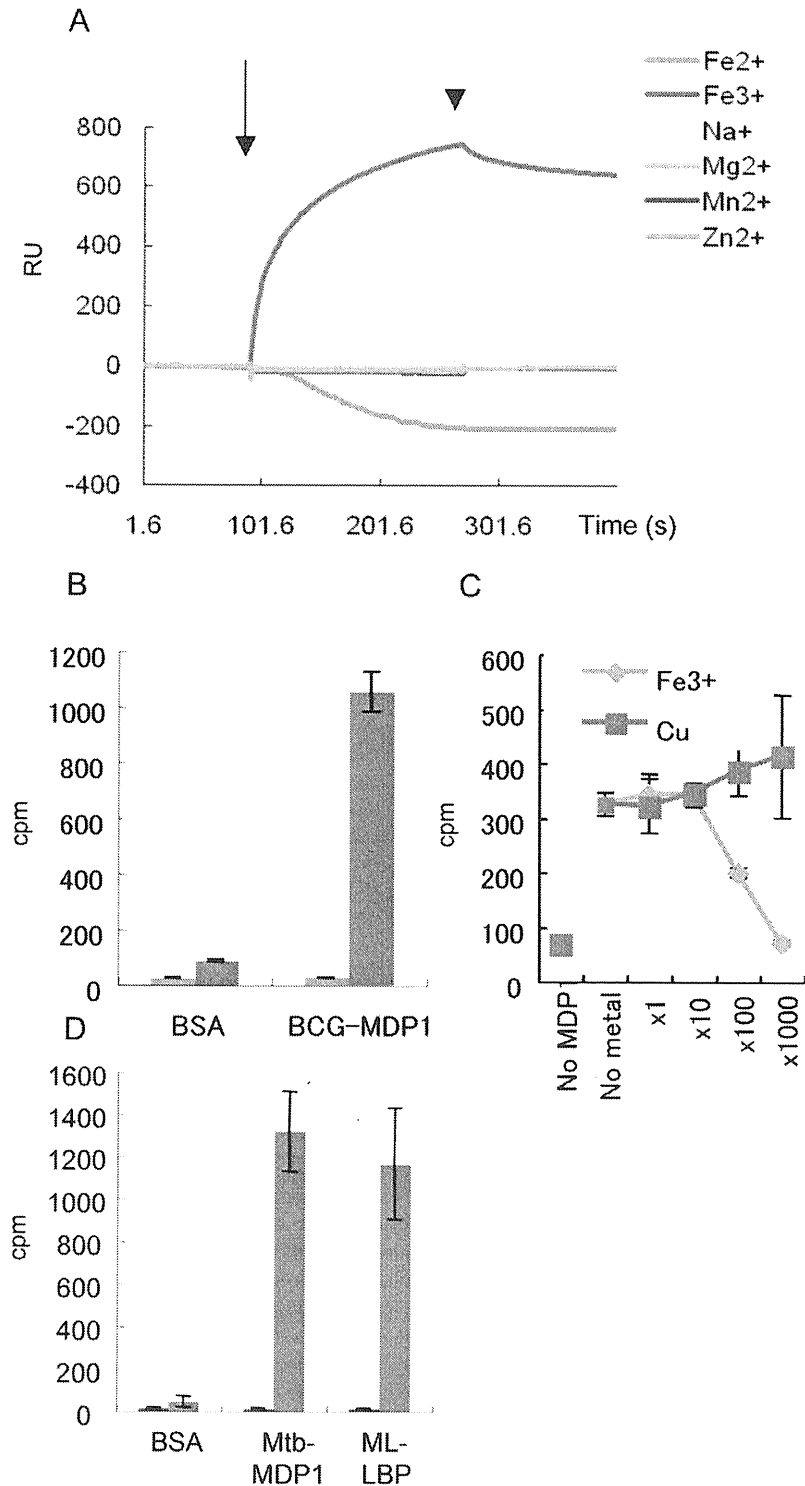
Figure 1. MDP1 binds to Fe^{3+}. (A) SPR analysis by Biacore biosensor. Each metal (1 mM) was loaded into the sensor, where BCG-MDP1 was immobilized. The SPR responses (RU, resonance units) subtracted from the MDP1-free sensor are presented. Arrow, starting point of injection of metals. Arrow head, stopping point of metal injection. Horizontal axis, time (seconds). (B) Protein-^{55}Fe interaction. Bovine serum albumin (BSA) or BCG-MDP1 was coated on a 96-well plastic plate. One μCi of ^{55}FeCl$_3$ was added to each well with (green bars) or without (red bars) incubation in 10 mM ascorbic acid. The level of bound iron was counted using a scintillation counter. Vertical axis, cpm (counts per minutes) of ^{55}Fe. (C) Inhibition of MDP1-^{55}Fe interaction by cold Fe^{3+}. One μCi of ^{55}FeCl$_3$ was added to the BCG-MDP1 coated or non-coated wells in the presence or absence of various molar concentrations of Fe^{3+} or Cu^{2+} as indicated. Vertical axis, level of bound ^{55}Fe. (D) Protein-^{55}Fe interaction. BSA, Mtb-MDP1, or ML-LBP was coated on a 96-well plastic plate. One μCi of ^{55}FeCl$_3$ was added to each well with (green bars) or without (red bars) incubation in 10 mM ascorbic acid. Levels of bound iron were counted using a scintillation counter.
doi:10.1371/journal.pone.0020985.g001

Table 1. Iron contents determined by ICP-MS.

Samples	(µg/kg)	Iron atoms/protein
BCG-MDP1	90.0	0.6
Buffer alone	155.0	ND
Iron-loaded BCG-MDP1	10,660.0±2505.6	81.4±19.1
Iron-loaded Mtb-MDP1	18,166.7±138.7	138.7±35.5

ND, not detected.
doi:10.1371/journal.pone.0020985.t001

generated in the presence of 1 mM H_2O_2 and 25 or 50 µM $FeSO_4$ by the Fenton reaction was monitored by "8-amino-5-chloro-7-phenylpyrido[3,4-d]pyridazine-1,4-(2H,3H) dione" (L-012), which reacts with reactive oxygen species and develops strong chemiluminescence (CHL) [26]. Hydroxyl radical was generated depending on the concentration of Fe^{2+} (Fig. 4A). In this experimental setting, the addition of 3 µM BCG-MDP1 remarkably suppressed the generation of hydroxyl radical (Fig. 4A). Furthermore, the addition of BCG-MDP1 after initiation of the Fenton reaction suppressed the production of hydroxyl radical even under optimal generating conditions (Fig. 4B). Similarly, both Mtb-MDP1 and ML-LBP suppressed the generation of hydroxyl radical by the Fenton reaction (Fig. 5). In contrast, neither histone H1 nor 3 µM BSA suppressed the Fenton reaction (Fig. 4A & B). Furthermore, the suppressive activity of 3 µM Mtb-MDP1 or ML-LBP was equivalent to 30 µM of the antioxidant sugar, ascorbic acid (data not shown).

Hydroxyl radical can be generated in the presence of bivalent metals other than iron and H_2O_2. In order to clarify whether the suppressive effect on the Fenton reaction by MDP1 is dependent on its ferroxidase activity, we studied the effects of BCG-MDP1 on Cu^{2+}-dependent Fenton-like reactions. For these studies hydroxyl radical was generated in the presence of 25 or 50 µM $CuSO_4$ and 1 mM H_2O_2 (Fig. 4C). The data showed that neither MDP1 nor histone H1 suppressed Cu^{2+}-induced Fenton-like reactions, but in fact enhanced the reaction. These data reinforce the hypothesis that inhibition of iron-induced Fenton reactions by MDP1 is indeed dependent on ferroxidase activity.

Dual mechanism of DNA protection by MDP1/ML-LBP

We next examined the effect of MDP1 on the protection of DNA. First, plasmid DNA (pUC19) was incubated with DNase1 in the presence or absence of 3 µM BCG-MDP1 and histone H1. We found that DNA was protected equally by MDP1 and histone H1 (Fig. 6A). Thus, both MDP1 and histone H1 protect DNA from DNase1 by acting as physical shields.
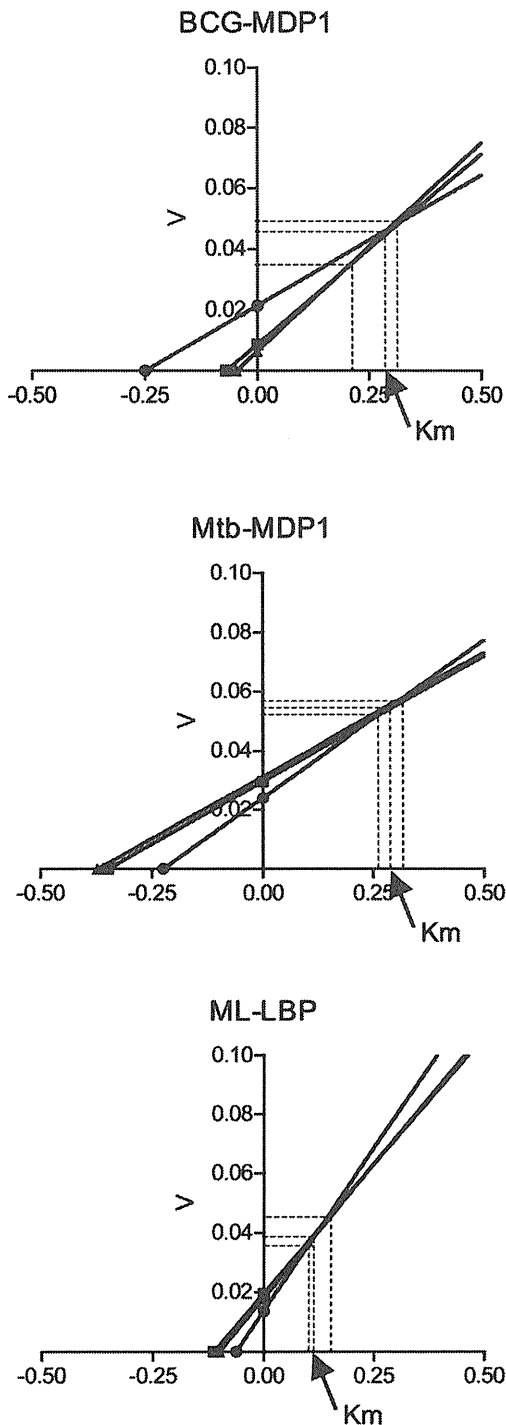
Comparison of the effects of MDP1 and histone H1 on DNA damage induced by the Fenton reaction revealed that DNA was degraded in the presence of 25 or 50 µM $FeSO_4$ and 1 mM H_2O_2 (Fig. 6B). BCG-MDP1 protected DNA from degradation by the Fenton reaction, whereas the level of protection exerted by histone H1 was comparatively lower (Fig. 6B). By contrast, neither BCG-MDP1 nor histone H1 could protect DNA from Cu^{2+}-induced Fenton-like reactions (Fig. 6C), further suggesting that MDP1 protects DNA by suppressing iron-induced Fenton reactions mediated through its ferroxidase activity. As expected both Mtb-MDP1 and ML-LBP also protected DNA from digestion with DNase1 and the damage caused by the Fenton reaction in a similar manner to BCG-MDP1 (Fig. 6D). Taken together, these data suggest that MDP1 and ML-LBP protect DNA in a dual fashion, by acting as a physical barrier and minimizing the Fenton reaction.
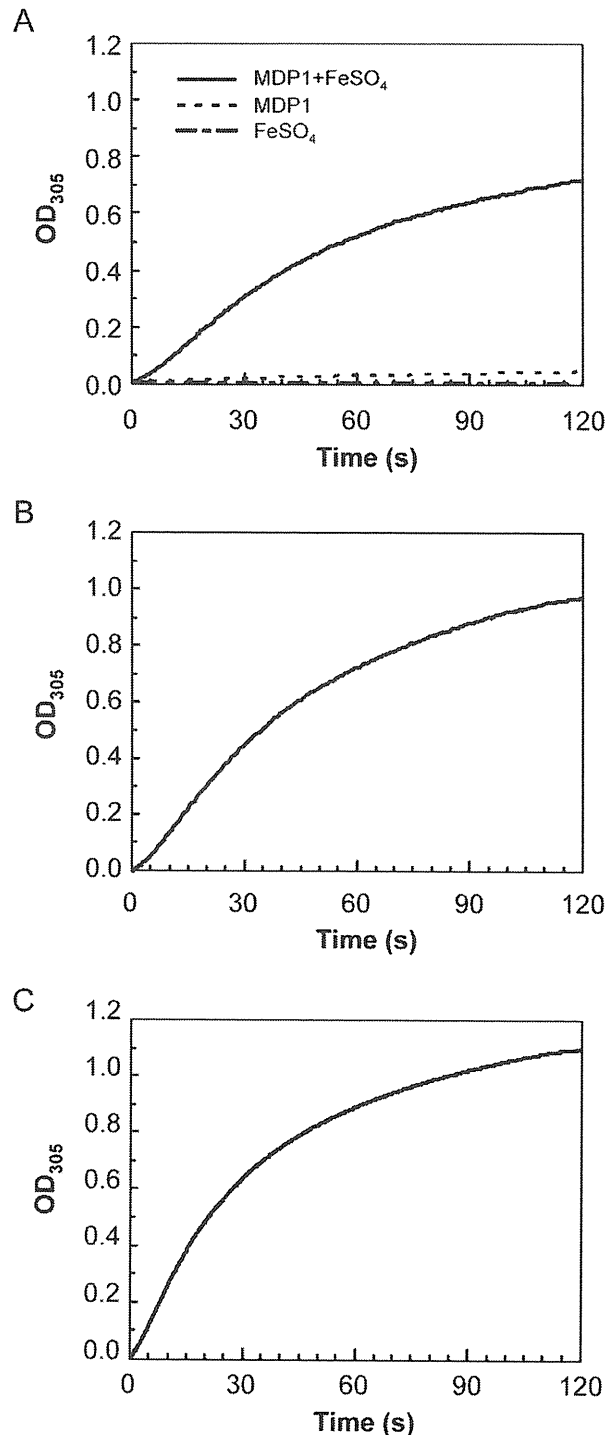
Figure 2. Ferroxidase activity of MDP1/ML-LBP. The conversion from Fe^{2+} to Fe^{3+} was determined by measuring the absorbance at 305 nm. (A) broken line, 1.4 µM BCG-MDP1; dush-dotted line, 0.4 mM $FeSO_4$; solid line, 0.4 mM $FeSO_4$+1.4 µM BCG-MDP1. (B) solid line, 0.4 mM $FeSO_4$+1.4 µM Mtb-MDP1. (C) solid line, 0.4 mM $FeSO_4$+1.4 µM ML-LBP. The reaction was monitored for 120 seconds.
doi:10.1371/journal.pone.0020985.g002

The role of MDP1 in the detoxication of iron in *Mycobacterium*

Finally, we assessed the role of MDP1 in the detoxication of iron in *Mycobacterium* itself. MDP1 is presumed to be essential for slow

BCG-MDP1

0.10
0.08
0.06
> 0.04
0.02

-0.50   -0.25   0.00   0.25   0.50

Km

Mtb-MDP1

0.10
0.08
0.06
> 0.04
0.02

-0.50   -0.25   0.00   0.25   0.50

Km

ML-LBP

0.10
0.08
0.06
> 0.04
0.02

-0.50   -0.25   0.00   0.25   0.50

Km

Figure 3. Ferroxidase activity of BCG-MDP1, Mtb-MDP1, and ML-LBP. The conversion from Fe^{2+} to Fe^{3+} was monitored by spectral analysis at 305 nm. 0.0125–0.1 mM $FeSO_4$ were added to 1.4 µM BCG-MDP1 (A), Mtb-MDP1 (B) and ML-LBP (C). Direct linear plots were shown by the straight lines intercepting X-axis with $-1/K_m$. K_m are taken as the median value from each series.
doi:10.1371/journal.pone.0020985.g003

growers of mycobacteria, such as BCG and *M. tuberculosis* [27,28] and cannot be knocked out. Therefore we employed the MDP1-homologue (Ms-MDP1)-deficient strain of rapid grower *Mycobacterium smegmatis* [29]. We detected the ferroxidase activity of purified Ms-MDP1, of which the K_m value was 0.136 mM (Figure

S2). We compared the resistance to H_2O_2 among wild type and mutant strains of *M. smegmatis*, including Ms-MDP1-deficient, and Ms-MDP1-complemented strains. These strains were treated with 12.5 mM H_2O_2 in the logarithmic phase of growth and the survival rate was determined by a colony forming unit (CFU) assay. There was a 100-fold reduction in survival of the Ms-MDP1-deficient strain (Fig. 7). We also pretreated bacteria with 40 mM desferal, an iron chelator. This treatment remarkably inhibited the bactericidal effect of H_2O_2 (Fig. 7), showing that major bactericidal effect with H_2O_2 treatment is depending on the Fenton reaction. Together, our data show that MDP1 play a role in iron detoxfication and bacterial survival.

Phylogenetic analysis of MDP1/ML-LBP homologues and ferritin-superfamily proteins

We accomplished molecular evolutionary analysis to recognize the phylogenetic diversity of MDP1/ML-LBP homologues and ferritin-superfamily proteins. We constructed phylogenetic dendrogram of MDP1/ML-LBP homologues and ferritin-superfamily proteins (bacterioferritin and Dps) of mycobacteria, such as BCG, *M. tuberculosis*, *Mycobacterium avium*, *Mycobacterium avium* subsp. *paratuberculosis*, *M. smegmatis*, and *M. leprae*. We also applied amino acid sequences of other bacterial ferritin-superfamily proteins of *E. coli*, *Salmonella enterica*, *Yersinia pestis*, and *Helicobacter pylori* and the dendrogram was created using clustering with the Unweighted Pair Group Method with Arithmetic Mean (UPGMA) by GENETYX software (Genetyx, Tokyo, Japan). In the phylogenetic tree (Figure 8), MDP1/ML-LBP homologues formed different cluster from ferritin-superfamily proteins, supporting phylogenetic distinctiveness between MDP1/ML-LBP homologues and ferritin superfamily proteins.
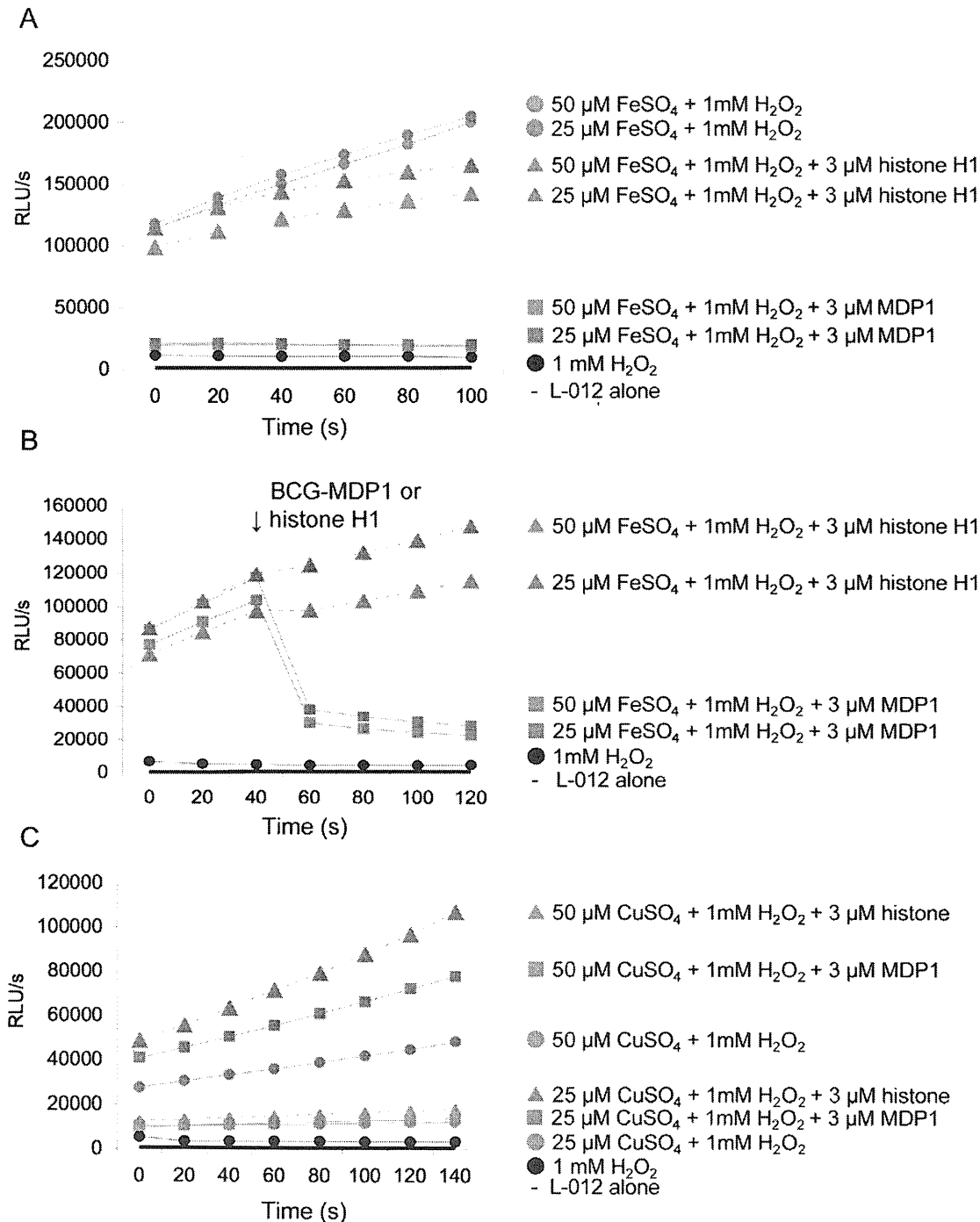
Discussion

Iron in living organisms is a double-edged sword, as it is an essential and beneficial element but is also harmful. Therefore, living organisms strictly control iron homeostasis. The ferritin superfamily proteins are distributed across all three domains of life and contribute to iron detoxication through oxidation and storage as Fe^{3+}, the nontoxic form of iron. Bacteria produce two types of ferritin superfamily proteins, one is bacterioferritin and another is Dps (also called miniferritin). Bacterioferritin is distributed among mycobacteria [12,13,30–32] but pathogenic mycobacteria, such as *M. tuberculosis* complex and *M leprae*, lack DNA-binding ferritin superfamily proteins like Dps. Here we show a histone-like mycobacterial protein, MDP1/ML-LBP has similar activity with ferritin superfamily proteins and protect DNA by preventing the Fenton reaction.

MDP1/ML-LBP is a major cellular component of mycobacterial cell [17,18] and is a multifunctional molecule depending on interaction with biomolecules, such as DNA, laminin [18,33], glycosaminoglycans [19,33], and glycolipids [22,28], and in turn controls gene expression, infection, and cell wall integrity [19,22,23,28,33]. In contrast, in this study, we identified enzymatic activity of MDP1 itself that should be involved in iron-homeostasis of mycobacteria.

This study was initiated by the unexpected detection of the increase and decrease of SPR, when Fe^{3+} and Fe^{2+} were loaded into BCG-MDP1-immobilized sensors, respectively (Fig. 1A). Because altered protein structure changes RU of SPR [25], we examined whether MDP1 actually binds to iron. We have shown that BCG-MDP1 binds to Fe^{3+}, but not to Fe^{2+} (Fig. 1B and C) and captures 81.4 ± 19.1 iron atoms/protein, as measured by ICP-MS (Table 1). We also confirmed similar iron-binding activity of recombinant Mtb-MDP1 and ML-LBP (Fig. 1D). MDP1 is eluted in the 150–

A

Legend (A):
- ○ 50 μM $FeSO_4$ + 1mM H_2O_2
- ● 25 μM $FeSO_4$ + 1mM H_2O_2
- △ 50 μM $FeSO_4$ + 1mM H_2O_2 + 3 μM histone H1
- ▲ 25 μM $FeSO_4$ + 1mM H_2O_2 + 3 μM histone H1
- ▦ 50 μM $FeSO_4$ + 1mM H_2O_2 + 3 μM MDP1
- ▦ 25 μM $FeSO_4$ + 1mM H_2O_2 + 3 μM MDP1
- ● 1 mM H_2O_2
- - L-012 alone

B

BCG-MDP1 or
↓ histone H1

Legend (B):
- △ 50 μM $FeSO_4$ + 1mM H_2O_2 + 3 μM histone H1
- ▲ 25 μM $FeSO_4$ + 1mM H_2O_2 + 3 μM histone H1
- ▦ 50 μM $FeSO_4$ + 1mM H_2O_2 + 3 μM MDP1
- ▦ 25 μM $FeSO_4$ + 1mM H_2O_2 + 3 μM MDP1
- ● 1mM H_2O_2
- - L-012 alone

C

Legend (C):
- ▲ 50 μM $CuSO_4$ + 1mM H_2O_2 + 3 μM histone
- ▦ 50 μM $CuSO_4$ + 1mM H_2O_2 + 3 μM MDP1
- ● 50 μM $CuSO_4$ + 1mM H_2O_2
- ▲ 25 μM $CuSO_4$ + 1mM H_2O_2 + 3 μM histone
- ▦ 25 μM $CuSO_4$ + 1mM H_2O_2 + 3 μM MDP1
- ● 25 μM $CuSO_4$ + 1mM H_2O_2
- ● 1 mM H_2O_2
- - L-012 alone

Figure 4. MDP1 suppresses the generation of the hydroxyl radical by the Fenton reaction. The hydroxyl radical level was measured by a L-012 probe sensitive to oxygen radicals. L-012 probe was added in all samples. RLU, relative luminescence units. (A) Proteins were added at the initiating time point of the Fenton reaction by H_2O_2 and $FeSO_4$. (B) Proteins were added 40 seconds after initiating the Fenton reaction. (C) The effect of proteins on the Fenton like reaction generated by H_2O_2 and $CuSO_4$.
doi:10.1371/journal.pone.0020985.g004

210 kDa fraction by gel filtration [17], suggesting that 7–10 MDP1 subunits oligomerize. Thus, it is estimated that oligomerized MDP1 can sequester 532–760 iron molecules, which is comparable to the iron-storage activity of ferritin superfamily proteins. The reduction of RU of SPR, when Fe^{2+} was injected into MDP1-immobilized sensor might be due to structural change of MDP1.

MDP1/ML-LBP is phylogenetically distinctive protein from ferritin superfamily proteins as shown in Figure 8. A remarkable difference in the method of iron storage between MDP1 and ferritin is that MDP1 directly captures Fe^{3+}, while ferritin incorporates iron after oxidizing Fe^{2+} using oxygen or hydrogen peroxide at the ferroxidase center. Thus, ferroxidase activity is dispensable for iron sequestration by MDP1/ML-LBP but not by ferritin superfamily proteins. These data suggest that MDP1/ML-LBP is a new type of iron detoxication and storage protein. The ferroxidase activity of MDP1 using O_2 as oxidant was slightly

- 94 -
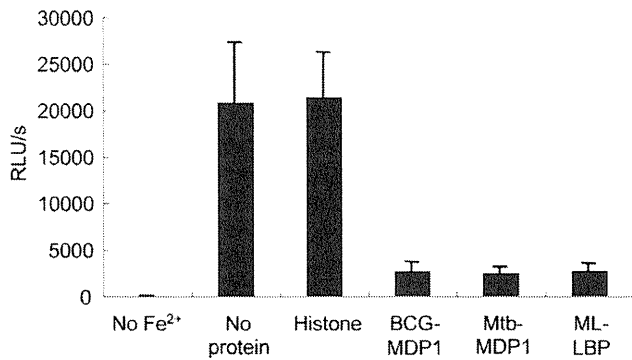
Figure 5. Mtb-MDP1 and ML-LBP suppress the generation of the hydroxyl radical by the Fenton reaction. The level of hydroxyl radical produced by the Fenton reaction was monitored using L-012, a probe that is sensitive to reactive oxygen, in the presence or absence of 3 µM proteins, such as bovine histone H1 (Histone), BCG-MDP1, Mtb-MDP1, and ML-LBP. The level of hydroxyl radical 10 sec after initiation of the reaction is shown. The data is representative of 3 independent experiments.
doi:10.1371/journal.pone.0020985.g005

slower but comparable with that of apo-horse ferritin (K_m value, 0.2127 mM) as shown in Figure S3. Taken together, to our knowledge, this is the first report of a molecule possessing iron oxidation and storage other than ferritin superfamily proteins.

The amino acid sequence of MDP1/ML-LBP resembles histones in eukaryotes and histone-like proteins in bacteria, thus it probably has a similar molecular root with those proteins. It is intriguing how MDP1/ML-LBP has evolved to acquire similar activity as ferritin superfamily proteins during evolution.

Mycobacteria are successful pathogens, producing various kinds of effector molecules that facilitate the long-term survival in the host. Acquisition of iron and preventing iron-dependent generation of ROS are essential events for the replication and survival in the host for the pathogens [9,34,35]. Dps is involved in the survival of bacterial pathogens, such as *Listeria* and *Salmonella*, by detoxifying iron [36]. Here we showed that Ms-MDP1 plays a critical role in iron detoxication in *M. smegmatis*, which produces Dps (Fig. 7). Therefore, it is reasonable to consider that MDP1/ML-LBP has more significant roles in the live and virulence of pathogenic mycobacteria, which lack Dps. That may be one of reasons why MDP1 is essential in *M. tuberculosis* [27]. Recent study conducted by Kumar et al, showing protection of DNA by MDP1
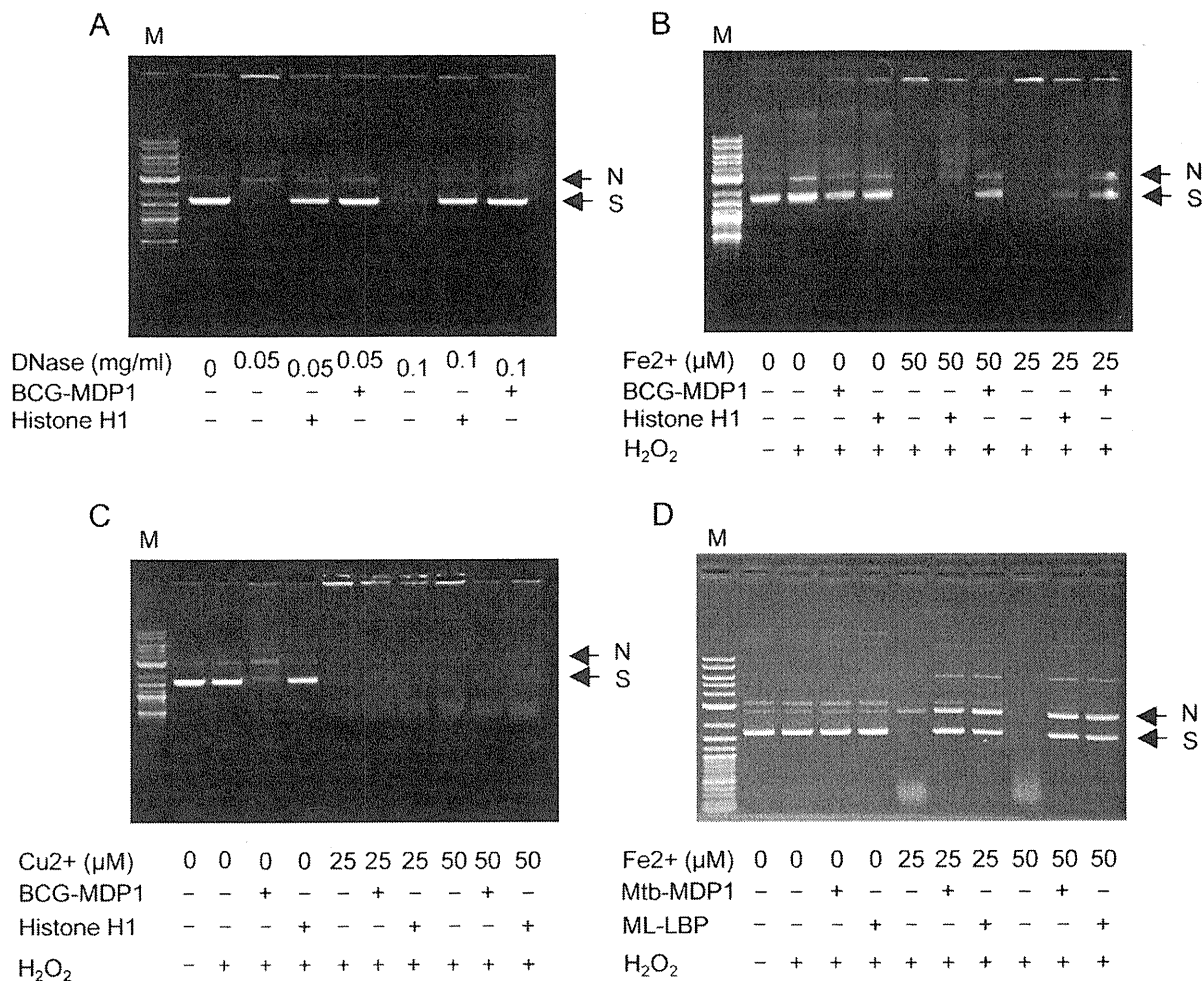
Figure 6. DNA protective activity of MDP1/ML-LBP. The plasmid DNA (pUC19) was treated with DNase 1 (A), H_2O_2 and $FeSO_4$ (Fenton reaction, B and C), and H_2O_2 and $CuSO_4$ (Fenton-like reaction, D) in the presence or absence of proteins, such as histone H1, BCG- MDP1, Mtb-MDP1, and ML-LBP. After reaction for 30 min, DNA was extracted, fractionated with gel electrophoresis and visualized by UV light after staining with ethidium bromide. M, marker. N, nicked DNA. S, supercoiled DNA.
doi:10.1371/journal.pone.0020985.g006
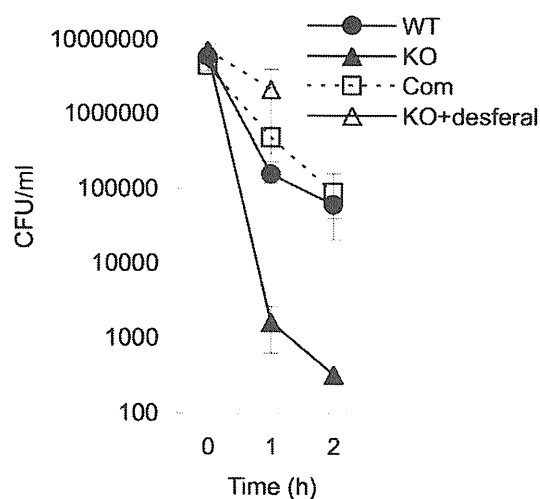
Figure 7. MDP1-deficient *M. smegmatis* is susceptible to H₂O₂ treatment. Bacteria at an exponential growth phase were treated with 12.5 mM H₂O₂ and the survival rate was determined by CFU. Closed circle, the wild-type *M. smegmatis* (WT). Closed triangle, MDP1-deficient *M. smegmatis* (KO), Open square, Ms-MDP1-complemented strain (Com). Open triangle, the MDP1-deficient strain pretreated with 40 mM desferal to confirm that iron is involved in the killing by H₂O₂ treatment (KO+desferal).
doi:10.1371/journal.pone.0020985.g007

from DNase 1 and the Fenton reaction, also support our finding [37]. Our finding on the new type of iron detoxication and storage protein will provide important information on the strategy and insight into virulence of mycobacteria.

Methods

Bacterial strains and proteins

MDP1-deficient *Mycobacterium smegmatis* was a gift from Dr. Thomas Dick [29]. The complemented strain was generated previously [22]. BCG-MDP1 and *M. smegmatis*-MDP1 (Ms-MDP1 or HLP) was purified from cultured BCG Tokyo and *M. smegmatis* mc²155, respectively, on Sauton media according to the method described previously [17]. Bovine histone H1 and bovine serum albumin (BSA) were purchased from Roche and Sigma, respectively. The open reading flame of MDP1 was amplified from the *M. tuberculosis* H37Rv genome using the following primers, forward: 5′-ccc cat atg aac aaa gca gag ctc att gac-3′, reverse: 5′-ccc aag ctt ttt gcg acc ccg ccg agc gg-3′, containing the restriction sites of NdeI and HindIII. The 645 bp amplicon was cloned into pCR2.1-TOPO (Invitrogen, Carlsbad, CA) and further subcloned as an NdeI-HindIII fragment in the corresponding site of pET-22b (+) (Novagen, Darmstadt, Germany). The plasmid was transformed and expressed in the *Escherichia coli* BL-21 strain and Mtb-MDP1 (Rv2986c) was purified using Ni-NTA agarose (Qiagen, Valencia, CA) with 300 mM imidazole in phosphate buffer (pH 7.4) after obtaining acid soluble proteins [17]. The *M. leprae*-MDP1 (ML-LBP or ML1683) was purified in the same way utilizing a previously constructed expression vector [18]. Concentrations of proteins were determined by Bradford's method [38] using BSA as a standard.

SPR analysis by Biacore biosensor

The interaction between BCG-MDP1 and metal was monitored by measuring SPR using a BIAcore 2000 biosensor (GE Healthcare, Buckinghamshire, UK). All binding reactions were performed at 25°C in 10 mM HEPES buffer, pH 7.4, including

150 mM NaCl, 1% BSA, 3 mM EDTA, and 0.005% surfactant P20 (HBSEP buffer). BCG-MDP1 was immobilized to the dextran matrix on the CM5 sensor chip (GE) using an amine coupling kit according to the manufacturer's instructions (GE). Metals, such as ammonium iron (III) citrate, CuSO₄, MgSO₄, MnCl₂, ZnSO₄, and FeSO₄, were dissolved in HBSEP buffer to a final metal ion concentration of 1 mM and injected over both the control and BCG-MDP1-immobilized sensor chip.

Detection of MDP1-⁵⁵Fe interaction

A 96-well ELISA plate (Sumitomo, Tokyo, Japan) was coated overnight with 5 µg/ml BCG-MDP1, Mtb-MDP1, ML-LBP or BSA in borate-buffered saline (pH 9.2) at 4°C. The wells were then washed with phosphate buffered saline (PBS). One hundred µl of PBS containing 1 µCi of ⁵⁵FeCl₃ (PerkinElmer, Boston, MA) was added into the wells coated with the proteins. In some cases, ⁵⁵FeCl₃ was incubated in 10 mM ascorbic acid for 30 min before addition to the wells. After 30 min incubation, the wells were washed four times in PBS containing 0.05% Tween 20. Then pre-warmed water at 37°C containing 1% SDS and 10 mM cold ammonium iron (III) citrate was added and the wells were flushed by pipetting. Twenty µl of the suspension was then spotted onto Whatman 3 MM paper and its radioactivity was counted by a liquid scintillation counter (Aloka, Tokyo, Japan).

### Inductively coupled plasma mass spectrometry (ICP-MS) analysis

After a heparin column was washed out with 10 mM sodium phosphate (pH 7), 1 ml of 0.1 mg/ml BCG-MDP1 or Mtb-MDP1 solution in pure water was incubated for 30 min. After washing, the column was incubated in the presence of 1 mM ammonium iron (III) (1 ml) citrate for 30 min. Unbound iron was washed out and the MDP1-iron complex was eluted by sodium phosphate buffer containing 2 M NaCl. Each sample of approximately 0.1 g was weighed accurately in quartz plates, and they were gradually carbonized with 0.5 ml of sulfuric acid using hot plates. They were then heated for 8 hours at 510°C in an electric furnace and finally washed. After cooling, the residue was dissolved with 1.25 ml of nitric acid and diluted to 25 ml with ultra pure water (the analysis solution). The Fe concentration of each analysis solution was determined by ICP-MS (Model ELAN DRC II; Perkin Elmer). We repeated the experiments 5 and 3 times for BCG-MDP1 and Mtb-MDP1, respectively.

Assay of ferroxidase activity

To determine whether MDP1 converts Fe²⁺ to Fe³⁺ using O₂ as oxidant, 0.4 mM FeSO₄ as 15 mM solution at pH 3.5 were added to 1.4 mM MDP1 in 20 mM Tris-HCl (pH 7.0) including with 150 mM NaCl. The protein solution was pre-incubated at 37°C for 10 min. UV spectral absorption at 305 nm has been traditionally used to monitor a µ-oxo-bridged Fe³⁺ dimmers, which was monitored by spectrophotometer U-3000 (HITACHI, Tokyo, Japan). MDP1 produced no UV absorbance in the absence of Fe²⁺. Lineweaver-Burk plot was used for considering the inverse values of the absorption per 60 s after addition of 0.0125–0.1 mM FeSO₄. The Kinetic parameters (K_m) were calculated by direct linear plot through the two points, K_m and V that satisfy the Michaelis-Menten equation exactly for every observation [39]. The best estimates, K_m was taken as the medians of the two sets of estimates.

Monitoring hydroxyl radical generation

Level of hydroxyl radical generation by the Fenton reaction were measured using L-012 (0.08 mM) as a probe as previously described [26]. The total reaction volume was 50 µl containing 20 mM Tris
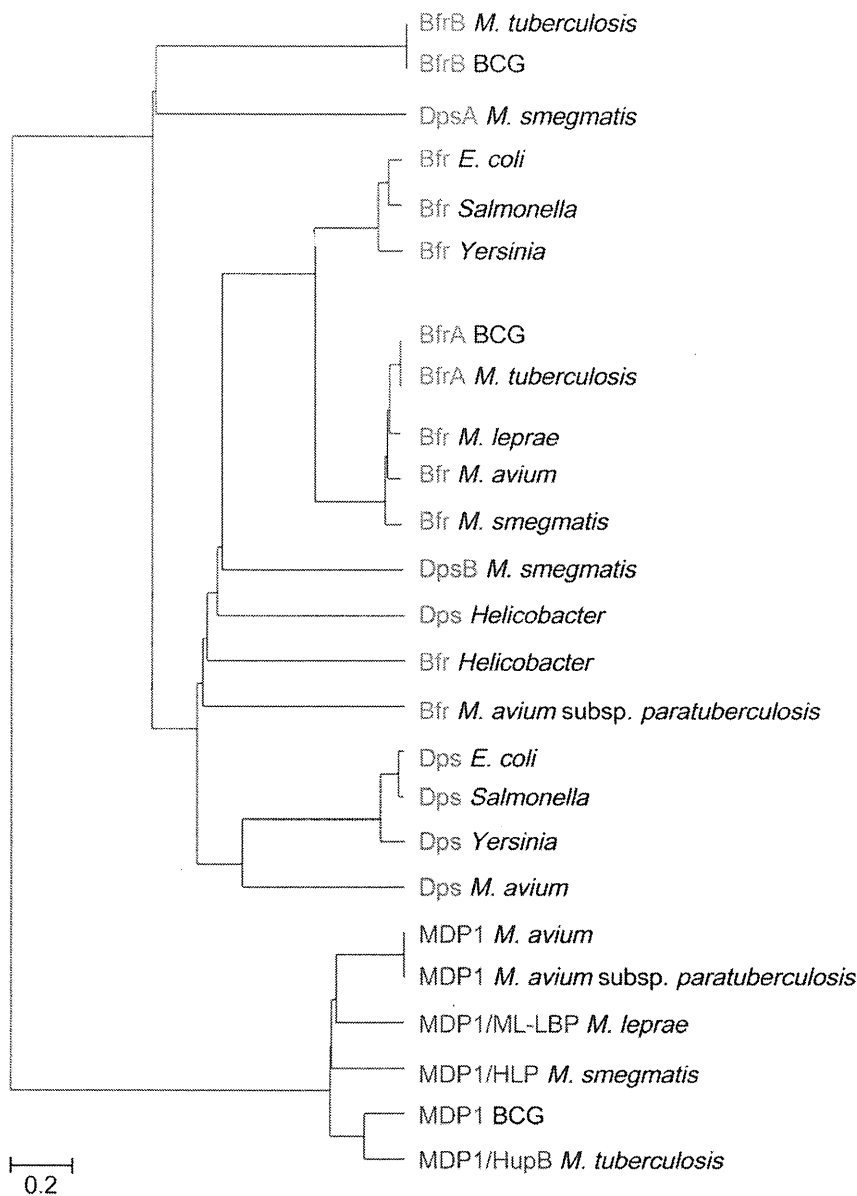
Figure 8. Phylogenetic tree of MDP1/ML-LBP homologues and ferritin superfamily proteins. The amino acid sequences of BCG-MDP1 (AB013441), *M. tuberculosis*-MDP1 (NP_217502), *M. avium*-MDP1 (YP_883003), *M. avium* subsp. *paratuberculosis* -MDP1 (NP_961958), *M. smegmatis*-MDP1 (YP_886729), *M. leprae*-ML-LBP (MDP1) (NP_302157), BCG-bacterioferritin A (BfrA) (YP_978002), BCG-BfrB (YP_979983), *M. tuberculosis*-BfrA (CAB10050), *M. tuberculosis*-BfrB (AAF06357), *M. avium*-Bfr (YP_882020), *M. avium* subsp. *paratuberculosis* (P45430), *M. smegmatis* Bfr (ABK70328), *M. leprae*-Bfr (AAA21339), *E. coli*-Bfr (AP_004454), *Salmonella enterica*-Bfr (CBY97651), *Yersinia pestis*-Bfr (AAS60481), *Helicobacter pylori*-Bfr (CAA06826), *M. avium*-Dps (YP_884099), *M. avium* subsp. *paratuberculosis*-Dps (NP_962494), *M. smegmatis*-DpsA (ABK75435), *M. smegmatis*-DpsB (ABK69831), *E. coli*-Dps (U00096.2), *Salmonella enterica*-Dps (Car32361.1), *Yersinia pestis*-Dps (AL590842.1), and *Helicobacter pylori*-Dps (1JI4_L) are compared by using Genetyx (Ver.16.1) software according to the UPGMA algorism. Values, 0.2, in the figure represent evolutionary distances.
doi:10.1371/journal.pone.0020985.g008

HCl (pH 7.5), 50 mM NaCl. Three μM Histone H1, BCG-MDP1, Mtb-MDP1, and ML-LBP were incubated with 25 or 50 μM FeSO$_4$ and 1 mM H$_2$O$_2$. After addition of L-012 (5 μl), CHL intensity was recorded continuously for 20–140 seconds using a Luminescence Reader BLR-201 (Aloka, Tokyo, Japan). The level of hydroxyl radical generation by the combination of 25 or 50 μM CuSO$_4$ and 1 mM H$_2$O$_2$ was monitored in the same way.

DNA protection assay

DNA protection from oxidative damage and enzymatic digestion was assessed *in vitro* using pUC19 plasmid DNA

(2686 bp, 50 nM), purified by a Qiaprep spin plasmid miniprep kit (Qiagen). The total reaction volume was 20 μl in pure water. Plasmid DNA was allowed to interact with MDP1, ML-LBP, or bovine Histone H1 for 30 min prior to the introduction of 25 or 50 μM FeSO$_4$ and 1 mM H$_2$O$_2$ or treatment with 50 or 100 μg/ml DNase I (Sigma, St.Louis, MO). The reaction mixtures were incubated for 30 min at room temperature before the reactions were stopped by incubation with 1% SDS and proteins were degraded by treatment with 20 μg/ml PronaseK (Sigma) for 30 min. Then the plasmid was extracted using phenol-chloroform extraction and 10 μl of sample was loaded on 1% agarose gel in

- 97 -